The temperature of the neutral hydrogen in the Galaxy

M.Sc. Thesis

By **Anushka Agarwal**



Department of Astronomy, Astrophysics and Space Engineering INDIAN INSTITUTE OF TECHNOLOGY INDORE May 20, 2025

The temperature of the neutral hydrogen in the Galaxy

M.Sc. Thesis

Submitted in partial fulfillment of the requirements for the awards of the degree

of
Master of Science

by **Anushka Agarwal**



Department of Astronomy, Astrophysics and Space Engineering INDIAN INSTITUTE OF TECHNOLOGY INDORE

May 20, 2025

Acknowledgements

First and foremost, I would like to express my sincere gratitude to my supervisor, Dr. Narendra Nath Patra, for giving me the opportunity to work on this project and for the supportive lab environment.

I would like to extend my sincere thanks to Dr. Nirupam Roy for his collaboration on this project and for the insightful discussions.

I am especially thankful to Abhinav Narayan for helping me learn the required software and for developing the pipeline used in this work. I also extend my appreciation to my labmates, Atharva, Keerthi, Harshal, Ashutosh, and Vatsal, for their constant support. I thank all my friends—Annie, Daisy, Vijay, Hari, Prasad, Parth, Gitaj, Navneet, Amardeep, Devesh, and Aryan for their support. I especially want to thank Vishrut for being a very good friend throughout this journey.

Finally, I acknowledge the resources and facilities provided by the Discipline of Astronomy, Astrophysics and Space Engineering at the Indian Institute of Technology Indore.



INDIAN INSTITUTE OF TECHNOLOGY INDORE

CANDIDATE'S DECLARATION

I hereby certify that the work which is being presented in the thesis entitled **The temperature of the neutral hydrogen in the Galaxy** in the partial fulfillment of the requirements for the award of the degree of MASTER OF SCIENCE and submitted in the DEPARTMENT OF ASTRONOMY, ASTROPHYSICS AND SPACE ENGINEERING, Indian Institute of Technology Indore, is an authentic record of my own work carried out during the time period from June 2024 to May 2025 under the supervision of Dr. Narendranath Patra, Assistant Professor, Department of Astronomy, Astrophysics and Space Engineering.

The matter presented in this thesis has not been submitted by me for the award of any other degree of this or any other institute.

Signature of the student with date ANUSHKA AGARWAL

This is to certify that the above statement made by the candidate is correct to the best of my/our

knowledge.

Nonendra North Patra.

14 05 2025

Signature of the Supervisor of M.Sc. thesis (with date)

DR. NARENDRANATH PATRA

ANUSHKA AGARWAL has successfully given his/her M.Sc. Oral Examination held on 06/05/2025.

Novendra North Patra.

Signature(s) of Supervisor(s) of MSc thesis

Date: 14/05/2025

Manoweta Chakrakosty Convenor, DPGC

Date: 19/05/2025

Mansueta Chakrakosty

Programme Coordinator, M.Sc.

Date: 19/05/2025

HoD, DAASE

Date:

Abstract

We present high-velocity resolution HI 21-cm absorption studies along 12 sightlines toward compact background radio sources, using the upgraded Giant Metrewave Radio Telescope (uGMRT). Our observations achieve an optical depth root mean square (RMS) noise of approximately 10^{-6} per kms⁻¹ velocity channel, enabling the detection of absorption features from the warm neutral medium (WNM). HI 21-cm absorption is detected along 10 of the 12 sightlines; no absorption is found toward 3C345 and 0023-236. For each sightline, we present the absorption spectra, the corresponding emission spectra from the Leiden-Argentine-Bonn (LAB) survey along nearby directions, and the derived spin temperature (T_S) spectra. In all cases, we detect maximum spin temperatures of $T_S \ge 10^3$ K, indicating that we are detecting the warm neutral medium.

Contents

Li	List of Figures		
Li	st of '	Tables	iii
1	Intr	roduction	1
	1.1	General Properties	2
	1.2	Multiphase Interstellar Medium	2
2	Rad	liative Transfer and the 21-cm line	6
	2.1	Observing the ISM: 21-cm transition of neutral hydrogen	6
	2.2	Radiative Transfer	9
3	Obs	servational Techniques	15
	3.1	Introduction	15
	3.2	The sample	16
	3.3	Observation	16
	3.4	Data Analysis	17
4	Resi	ults and Discussion	23
5	Con	nclusion	37
	5.1	Summary	37
	5.2	Future Scope	38

List of Figures

2.1	An illustration of the electromagnetic spectrum, showing the wavelength range and which frequencies penetrate the Earth's atmosphere. (Source: derivation of a Wikipedia and NASA image.)	7
2.2	Energy levels of the hydrogen atom (not to scale) showing hyperfine splitting and higher energy transitions	8
2.3	Illustration of the Radiative processes: absorption, spontaneous emission, and stimulated emission. The energy difference between the ground and excited states is $h\nu$. (Source: From lecture by Francesca Perrotta on Radiative Processes in Astrophysics)	10
3.1	Giant Meterwave Radio Telescope (GMRT)	18
3.2	Amplitude v/s time plot (from CASA) for a standard GMRT observation	19
3.3	Amplitude v/s time plot (from CASA) showing the frequency switching observation for the source 0010-418. The two colors correspond to the two spectral windows (SPW0 $\sim 1415 - 1421$, SPW1 $\sim 1417 - 1423$)	20
3.4	Amplitude v/s frequency plot (from CASA) after flagging and calibration. The plot shows the two spectral windows corresponding to two colours.	20
4.1	HI 21-cm absorption spectra obtained using the uGMRT. The top, middle, and bottom panels represent the 21-cm emission spectra (from the LAB Galactic survey), 21-cm optical depth spectra from our observation, and derived spin temperature spectra, respectively.	24
4.1	(Continued) HI 21-cm absorption, emission from LAB survey, and spin temperature spectra for source 2130	25
4.1	(Continued) HI 21-cm absorption, emission from LAB survey, and spin temperature spectra for source 0010	26

4.1	(Continued) HI 21-cm absorption, emission from LAB survey, and spin temperature spectra for source 2136	27
4.1	(Continued) HI 21-cm absorption, emission from LAB survey, and spin temperature spectra for source 0405	28
4.1	(Continued) HI 21-cm absorption, emission from LAB survey, and spin temperature spectra for source 0023	29
4.1	(Continued) HI 21-cm absorption, emission from LAB survey, and spin temperature spectra for source 0538	30
4.1	(Continued) HI 21-cm absorption, emission from LAB survey, and spin temperature spectra for source 0745	31
4.1	(Continued) HI 21-cm absorption, emission from LAB survey, and spin temperature spectra for source 1130	32
4.1	(Continued) HI 21-cm absorption, emission from LAB survey, and spin temperature spectra for source 1308	33
4.1	(Continued) HI 21-cm absorption, emission from LAB survey, and spin temperature spectra for source 1326	34
4.1	(Continued) HI 21-cm absorption, emission from LAB survey, and spin temperature spectra for source 3C345	35

List of Tables

1.1	General Properties of different phases of interstellar gas	3
3.1	Statistical parameters from the Kolmogorov–Smirnov Test evaluating the Gaussian nature of baseline residuals in off-line spectral channels for all observed sources	22
4.1	Summary of observational results	36

Acronyms

ATCA Australia Telescope Compact Array

CASA Common Astronomy Software Applications

CNM Cold Neutral Medium

GMRT Giant Metrewave Radio Telescope

HI Neutral Hydrogen

HIM Hot Ionized Medium

ISM Interstellar Medium

K-S Test Kolmogorov-Smirnov Test

LAB Leiden/Argentine/Bonn Galactic HI Survey

LO Local Oscillator

LSR Local Standard of Rest

Ly α Lyman-alpha

RFI Radio Frequency Interference

 T_B Brightness Temperature

 T_S Spin Temperature

VLA Very Large Array

WNM Warm Neutral Medium

WSRT Westerbork Synthesis Radio Telescope

Chapter 1

Introduction

Astrophysics, as defined in the dictionary, is a branch of astronomy that uses physical laws and principles to explain the behavior of stars and other objects in space ¹, which includes studying the *interstellar medium* as well. The process of star formation is closely linked to the interstellar medium of the galaxy. Studying star formation is extremely important in the field of astronomy and astrophysics for various reasons, one of which is to understand the evolution of galaxies. It is crucial to focus on understanding the condition of the ISM in order to understand star formation and, hence, the evolution of galaxies.

The interstellar medium, generally defined as "the medium between the stars," is not just a passive medium between celestial bodies but is the birthplace of stars and plays an important role in the galactic ecosystem. Star formation taking place from a primeval reservoir of gas is not totally efficient, and some residual gas is left behind, which constitutes the primary interstellar medium. Over time, this medium continuously exchanges matter and energy with stars by engaging in an ISM–star cycle. In this cycle, the star is first formed from the primary ISM, then, through processes such as supernova explosions, solar flares, etc., matter and energy are expelled into the ISM, which also produces turbulence. This may influence and give rise to more star-formation-prone regions, which are the cold, dense molecular

¹Cambridge-Dictionary-Online:https://dictionary.cambridge.org/dictionary/english/astrophysics

clouds. These processes connect the stellar scale processes to the galactic scales.

It was not until 1904 that astronomers discovered the existence of the interstellar medium. During a study by Hartmann 1904, stationary absorption lines of ionized calcium (Ca II) were discovered towards δ -Orionis. In a spectroscopic binary star, the spectral lines should exhibit periodic wavelength shifts due to the orbital motion. The presence of a stationary line was therefore taken as an indication of some intervening medium. Later, many other spectroscopic observations confirmed the existence of this matter in the Galaxy, now known as the interstellar medium.

1.1 General Properties

The primary constituents of the interstellar medium (ISM) are gas, dust, charged particles, and magnetic fields. ISM consists of relatively less mass (about $10 \sim 15\%$ of the galaxy's mass), but it shows dramatic variation in density and temperature. It plays a important role in the chemical and physical processes of the galaxy. The chemical composition of the ISM mirrors the overall composition of the universe. It contains hydrogen (70.4%), helium (28.1%), and small amount of other heavier elements (1.5%).

It has varying density and temperature ranges. Roughly half of the interstellar mass is confined in discrete clouds (mainly cold molecular clouds and cold atomic clouds) which takes only $\sim 1\text{-}2\%$ of interstellar space. The rest of the interstellar matter is in between these clouds. They are in warm neutral, warm ionized, and hot ionized phases. The general properties of different phases of the interstellar medium are in the table 1.1.

1.2 Multiphase Interstellar Medium

The foundational model of the interstellar medium (ISM) of the Galaxy posits that all its phases are in approximate thermal pressure equilibrium. In this picture, the high-density, cold neutral medium (CNM) is embedded within a lower-density, warm neutral medium (WNM), which in turn is embedded within an even lower-density, hot ionized medium (HIM) (McClure-Griffiths

Component of	Temperature	Density	Fractional
ISM	(K)	$n (cm^{-3})$	Volume
Cold molecular gas	10 – 20	$10^2 - 10^6$	≤ 1%
Cold neutral gas	50 – 100	20 - 50	1 – 5%
Warm neutral gas	6000 – 10000	0.2 - 0.5	10 – 20%
Warm ionised gas	~ 8000	0.2 - 0.5	20 - 50%
Hot ionised gas	~ 10 ⁶	~ 0.0065	30 – 70%

Table 1.1: General Properties of different phases of interstellar gas

Adapted from Ferrière 2001

2023). Observationally, multiple studies have confirmed that the ISM indeed consists of a cold, high-density phase, which produces narrow absorption features against background continuum sources, and a warm, low-density phase, which primarily contributes to emission and is difficult to detect in absorption due to its low optical depth. Theoretical models predict that, based on the balance of different heating and cooling processes in the ISM, two stable phases coexist: (1) the CNM, with typical densities of $n \sim 10$ –100 cm⁻³ and temperatures of $T \sim 50$ –200 K, and (2) the WNM, with densities of $n \sim 0.1$ –1 cm⁻³ and temperatures of $T \sim 6000$ –10000 K (Wolfire 1995). The theoretically expected temperatures of the CNM have been well understood and confirmed observationally (Roy 2006). The WNM, with its relatively high temperature and low optical depth, produces much broader absorption features that are challenging to detect; their detection typically requires high-velocity-resolution interferometric observations.

Many studies focused on measuring the temperature of the warm neutral phase of the ISM have found that the gas is in the thermally unstable range, suggesting that a significant fraction of the warm neutral medium (WNM) exists in an unstable thermal state. This finding has sparked considerable curiosity, as this questions the theoretical model of the ISM phases, which is the basis of our understanding. Heiles and Troland 2003 observed 79 compact radio sources using the Arecibo single-dish telescope, conducting HI 21-cm emission and absorption studies, and found that approximately

48% of the warm gas was in the thermally unstable temperature range. In this study, there is an underlying assumption that the HI cloud is homogeneous on a scale larger than that of the emission beam. A different approach was taken by Carilli 1998 and Dwarakanath 2002, who used interferometric HI studies to detect broad absorption features. A similar approach was used by Nissim Kanekar 2003, who conducted a high-velocity-resolution HI 21-cm absorption study using the Australia Telescope Compact Array (ATCA) towards two compact sources. This interferometric approach, targeting broad absorption features to detect the WNM, effectively resolved out the foreground HI emission problem, as it focused on compact point sources having a pencil-beam towards the continuum source. With all these studies, it has been established that high-velocity-resolution interferometric studies allow us to detect WNM corresponding to the broad absorption features by separating out narrow CNM components from the spectra.

A bigger project has been started by Nirupam Roy in 2013, aiming to detect the WNM in absorption and to determine its range of kinetic temperatures and the temperature distribution of neutral gas in the ISM of the Milky Way by conducting a high-velocity-resolution-interferometric HI 21-cm absorption study towards a large number of compact radio sources using the Giant Metrewave Radio Telescope (GMRT) and the Westerbork Synthesis Radio Telescope (WSRT). In the first papers of this bigger project, Roy 2013a and Roy 2013b reported a high-resolution HI 21-cm absorption study towards 32 compact radio sources observed from GMRT and WSRT. The optical depth spectra in this study have a root mean square noise value of 10^{-3} per km s^{-1} velocity channel width, which is sufficient for the detection of absorption by the warm neutral medium. They also observed a few sources from both the GMRT and WSRT to check for the spectral baseline problems. For one source, B0438 - 436, the absorption was not detected and it required more observational time; it was detected in a study by Patra 2018 (with observational time ~ 30 h). In the continuation of the first paper, Roy 2013b from the multi-gaussian decomposition of the absorption spectra reported that $\sim 28\%$ of the gas have temperature in the thermally unstable range. In work by Patra 2024, high-resolution absorption studies towards 12 WSRT compact radio sources line of sights has been conducted. It has

sufficient RMS noise in the optical depth spectra to detect WNM. In the continuation of this bigger project, in this thesis I am going to present the analysis of 12 sources observed from uGMRT with excellent sensitivity, and with very high resolution compared to any of the earlier studies.

Chapter 2

Radiative Transfer and the 21-cm line

Observation is essential for verifying theories, getting feedbacks and refining our understanding of the universe. Even though astronomy is one of the oldest sciences, the first observation of radio waves was made in 1933 by Karl Jansky (Jansky 1933). This opened a whole new window to the universe, offering a different perspective of observation. Radio astronomy concerns the part of the electromagnetic spectrum where $\nu \leq 300 \, \text{GHz}$, this corresponds to the wavelength $\lambda \geq 1 \, \text{mm}$, as shown in Figure 2.1. The frequency between 30 MHz and 30 GHz easily penetrates the atmosphere of the Earth, so it is possible to observe it from the ground. Since our target is far from us and these signals are often faint, a large amount of observations is required. In this chapter, the sections consist of information about 21-cm of neutral hydrogen, which is the most important tracer in the radio regime of the ISM, and about the radiative transfer required to infer the quantities from the HI 21-cm observations.

2.1 Observing the ISM: 21-cm transition of neutral hydrogen

In radio frequencies, the most useful tracer of the interstellar medium is the 21-cm line of neutral hydrogen. There are two reasons for its importance,

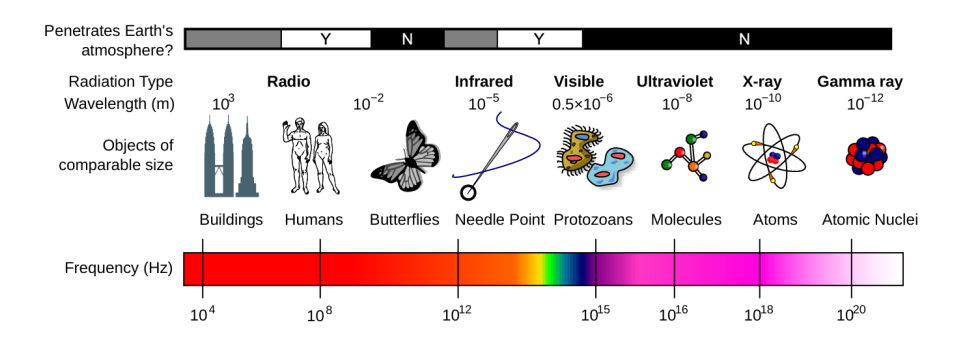
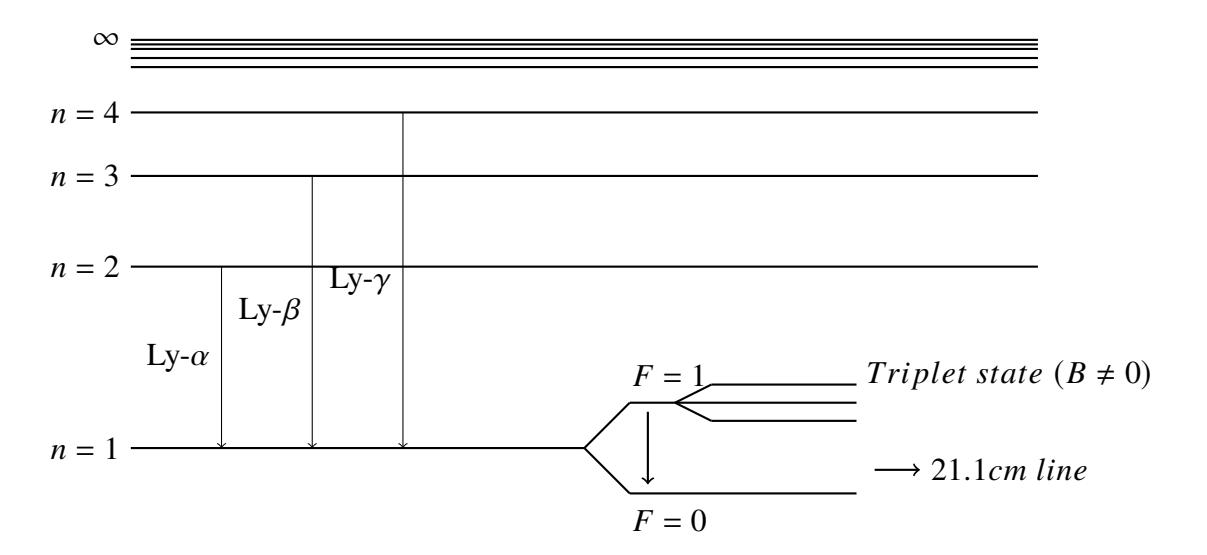


Figure 2.1: An illustration of the electromagnetic spectrum, showing the wavelength range and which frequencies penetrate the Earth's atmosphere. (Source: derivation of a Wikipedia and NASA image.)

one is the abundance of neutral hydrogen in the Galaxy, and the other is the possibility of extracting important quantities about the physical conditions in the ISM from the spectra. The existence of this line was theoretically predicted by Jan Hendrik van de Hulst in 1944, and it was observationally confirmed by Ewen and Purcell 1951.

The ground state of the neutral hydrogen (HI) atom is split into four hyperfine levels, as seen in the Figure 2.2. In the absence of an external magnetic field, three of these levels are degenerate and referred to as the triplet state, while the remaining one is called the singlet state. These configurations correspond to the total angular momentum quantum number F, with F=1 for the triplet state having parallel spins and F=0 for the singlet state having anti-parallel spins. Since the orbital angular momentum in the ground state is zero, the total angular momentum arises solely from the sum of the electron and proton spins. Due to the interaction between the magnetic moment of the electron and proton, the energy difference between these two states (triplet and singlet) emerges. The orientation of the magnetic moment in the triplet state is anti-parallel and in the singlet state parallel, with the triplet state having the higher energy. The energy difference between these two hyperfine states is equal to hv with v=1420.405752 MHz, corresponding to the 21.1 cm line of neutral hydrogen.

The probability of the transition of the electron from the triplet state to the singlet state is very low, about 2.85×10^{-15} s⁻¹. This implies that the natural



13.6 eV

Figure 2.2: Energy levels of the hydrogen atom (not to scale) showing hyperfine splitting and higher energy transitions

lifetime of the electron to emit the 21 cm line is about 10 million years, it is also called the forbidden line due to this reason. But due to the processes such as the collisional transition, existence of radiation at 21 cm, and the $Ly-\alpha$ pumping, the 21 cm transition occurs before the natural lifetime. In collisional and radiative transitions, the energy equal to hv is exchanged in order for the transition to take place. Processes such as excitation of an electron from one of the hyperfine levels of the ground state of HI to the higher level, followed by its de-excitation to another hyperfine level through $Ly-\alpha$ or higher Ly lines is also a possibility.

The number of atoms in the triplet state (n_1) and singlet state (n_0) is given by the equation 2.1, where g_1 and g_0 are the statistical weights given by g = 2F + 1. This means $n_1 = 3n_0 \exp(-h\nu/T_s)$, here T_s is called the spin temperature. It is a means of quantifying the number distribution between the two states. If we consider the total number of electrons here as n, then $n_0 = \frac{n}{4}$ and $n_1 = \frac{3n}{4}$.

$$\frac{n_1}{n_0} = \frac{g_1}{g_0} e^{-\frac{h\nu}{KT_s}} \tag{2.1}$$

Now that we've established the importance of the 21-cm line, we delve into the radiative processes that allow us to interpret the data from these observations.

2.2 Radiative Transfer

Radiative processes include absorption, spontaneous emission, and stimulated emission, as described in Figure¹ 2.3. Einstein's A and B coefficients describe and relate these three processes of interaction between radiation and matter, governing their probabilities. The rate of absorption is proportional to the number of atoms in the ground state (n_0) and the energy density (u_v) , and is given by $n_0u_vB_{01}$. The rate of spontaneous emission is proportional only to the number of atoms in the excited state (n_1) , given by n_1A_{10} . The rate of stimulated emission is proportional to both the number of atoms in the excited state (n_1) and the energy density (u_v) , given by $n_1u_vB_{10}$. Here A_{10} , B_{01} , B_{01} are Einstein's A and B coefficient. In thermodynamic equilibrium, a balance between these radiative processes must be achieved, leading to specific relationships among the Einstein coefficients.

$$A_{10} = \frac{8\pi h v^3}{c^3} B_{10} \tag{2.2}$$

$$g_0 B_{01} = g_1 B_{10} \tag{2.3}$$

For a more detailed description, the Einstein coefficients can be expressed in terms of microscopic cross-sections for absorption and emission (σ) , so the rate of absorption can be written as Eq.2.4. It is considered here that u_{ν} does not vary appreciably over the line profile of $\sigma_{01}(\nu)$.

$$\Gamma_{01}^{absorption} = n_0 \frac{cu_{\nu}}{h\nu} \int d\nu \, \sigma_{01}(\nu) \tag{2.4}$$

Also, as described above

$$\Gamma_{01}^{absorption} = n_0 u_{\nu} B_{01}$$

$$\Rightarrow B_{01} = \frac{c}{h\nu} \int d\nu \,\sigma_{01}(\nu) \tag{2.5}$$

Taking the value of B_{01} from the Eq.2.2 and Eq.2.3, and equating it with the Eq.2.5, we have

$$B_{01} = \frac{g_1}{g_0} \frac{c^3}{8\pi h v^3} A_{10}$$

https://people.sissa.it/~perrotta/lezioni_2023_2024/chapter10.
pdf

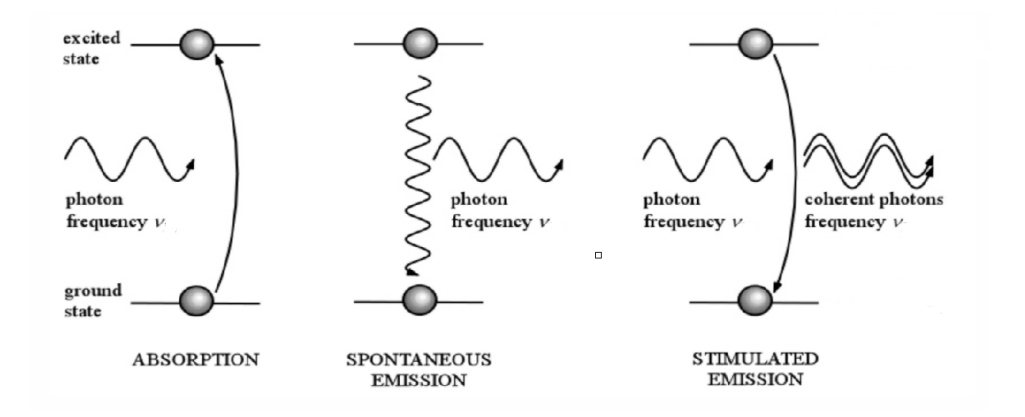


Figure 2.3: Illustration of the Radiative processes: absorption, spontaneous emission, and stimulated emission. The energy difference between the ground and excited states is $h\nu$. (Source: From lecture by Francesca Perrotta on Radiative Processes in Astrophysics)

$$\Rightarrow \int d\nu \, \sigma_{01}(\nu) = \frac{g_1}{g_0} \frac{c^2}{8\pi \nu^2} A_{10}$$

$$\Rightarrow \sigma_{01}(\nu) = \frac{g_1}{g_0} \frac{c^2}{8\pi \nu^2} A_{10} \phi_{\nu}$$
(2.6)

Here, we are relating the monochromatic absorption cross-section to a normalized line profile. Similarly, we will get the value for B_{10} and σ_{10} .

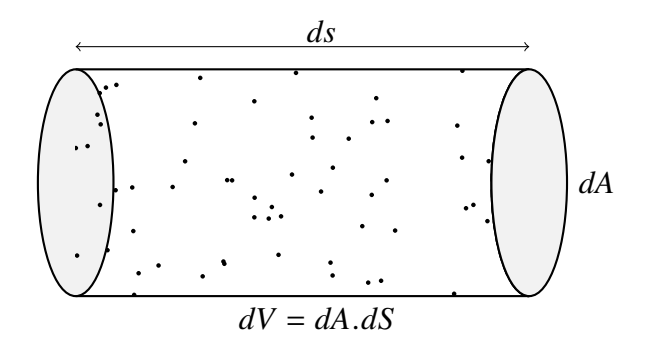
$$B_{10} = n_1 u_{\nu} \frac{c}{h\nu} \int d\nu \, \sigma_{10}(\nu) \tag{2.7}$$

$$\sigma_{10}(\nu) = \frac{c^2}{8\pi\nu^2} A_{10}\phi_{\nu} \tag{2.8}$$

From Eq.2.6 and Eq.2.8 we also have

$$\frac{\sigma_{01}}{\sigma_{10}} = \frac{g_1}{g_0} \tag{2.9}$$

This result is important for calculating the column density (N_{HI}) , before that we should understand the fundamentals of radiative transfer well. So to better understand the emission and absorption processes, we consider a simple geometrical model: a small cylinder of volume dV with cross-section dA and length dS, as shown in the diagram below.



Then the emission (only) from the particles will be given in terms of the emission coefficient j_{ν} , given in the equation below. The unit of j_{ν} is $Wm^{-3}s^{-1}Hz^{-1}Sr^{-1}$.

$$dE = dI_{\nu}dAdtd\nu d\Omega = j_{\nu}dV (= dAdS)d\nu d\Omega dt \qquad (2.10)$$

$$\Rightarrow dI_{\nu} = j_{\nu}dS \tag{2.11}$$

Here, dE is the total energy and I_{ν} is the specific intensity.

If we consider only the absorption by the particles inside the cylinder, then the initial intensity I_{ν} will be reduced by the absorption coefficient (α_{ν}) . Here α_{ν} is the denotion for the number per unit volume (n, cm^{-3}) of particles times its cross-sectional area (σ_{ν}, cm^{2}) , which is the effective area for absorption. These particles are distributed at random. The total number of particles, n, is given by ndAdS, and the total absorbing area is given by $n\sigma_{\nu}dAdS$. The unit of absorption coefficient (α_{ν}) is cm^{-1} .

$$dE = dI_{\nu}dAdtd\nu d\Omega = -I_{\nu}(n\sigma_{\nu}dAdS)d\nu d\Omega dt$$

$$\Rightarrow dI_{\nu} = -I_{\nu}(n\sigma_{\nu})dS$$

$$\Rightarrow dI_{\nu} = -I_{\nu}\alpha_{\nu}dS \qquad (2.12)$$

Taking into account both the emission and absorption, by combining the above expression 2.11 and 2.12. We get the radiative transfer equation 2.13.

$$\frac{dI_{\nu}}{dS} = j_{\nu} - I_{\nu}\alpha_{\nu} \tag{2.13}$$

By introducing the optical depth, defined as $\tau_{\nu} = \int_{0}^{l} \alpha_{\nu} dS$ with $d\tau_{\nu} = \alpha_{\nu}.dS$, where l is the total path length, Eq. 2.13 becomes:

$$\frac{dI_{\nu}}{d\tau_{\nu}} = S_{\nu} - I_{\nu} \tag{2.14}$$

Solving this equation, we get

$$I_{\nu} = I_{0} e^{-\tau_{\nu}} + \int_{0}^{\tau_{\nu}} S_{\nu} e^{-(\tau_{\nu} - \tau_{\nu}^{'})} d\tau_{\nu}^{'}$$
 (2.15)

where S_{ν} is the source function, defined as the ratio of emission coefficient and absorption coefficient and, I_0 is the inital imtensity. In the above Eq.2.15, the first term shows the initial intensity diminished by absorption, and the second term shows emission from each part and absorption from the rest. If the source function is constant, then

$$I_{\nu} = I_{\nu}(\tau_{\nu} = 0) e^{-\tau_{\nu}} + S_{\nu} (1 - e^{-\tau_{\nu}})$$
 (2.16)

If thermal equilibrium is present, then $S_{\nu} = B_{\nu}$. We also see that if $\tau >> 1$, then $I_{\nu} = B_{\nu}$. In radio regime, the intensity is calculated in terms of brightness temperature (T_B) .

$$I_{\nu} = \frac{2k\nu^2 T_B}{c^2} \tag{2.17}$$

According to Plank's law, we have

$$B_{\nu}(T) \equiv \frac{2h\nu^3}{c^2} \cdot \frac{1}{e^{h\nu/kT} - 1}$$
 (2.18)

If we use Eqs. 2.17 and 2.18 with $\frac{h\nu}{kT} \ll 1$, then Eq.2.16 takes the below form

$$T_B = T_B(0) e^{-\tau_{\nu}} + T (1 - e^{-\tau_{\nu}})$$
 (2.19)

For an isothermal HI cloud with no background source,

$$T_B = T_S (1 - e^{-\tau_{\nu}}) \tag{2.20}$$

For optically thin limit, $hv/kT \ll 1$

$$T_B = T_S . \tau_{\nu} \tag{2.21}$$

To derive column-density (N_{HI}) , let us first consider the attenuation coefficient (κ)

$$\kappa_{\nu} = n_0 \sigma_{01} - n_1 \sigma_{10}$$

Using Eq.2.9 and Eq.2.1,

$$\kappa_{\nu} = \frac{3c^2}{32\pi h \nu^3} n A_{10} \phi_{\nu} \frac{h\nu}{kT_s}$$
 (2.22)

The optical depth is,

$$\tau = \int \kappa_{\nu} dS$$

$$\Rightarrow \tau = \frac{3c^2}{32\pi h \nu^3} A_{10} \phi_{\nu} \frac{h\nu}{kT_s} \int ndS$$

$$\Rightarrow \tau = \frac{3c^2}{32\pi h \nu^3} A_{10} \phi_{\nu} \frac{h\nu}{kT_s} N_{HI}$$

For the optically thin approximation ($\tau \ll 1$), the line-of-sight column density of neutral hydrogen (N_{HI}), which represents the integrated number density along the sightline, can be measured from HI 21-cm emission studies (e.g., Kulkarni and Heiles 1988, Dickey and Lockman 1990). In the following equations, N_{HI} is in units of cm⁻², and the velocity V is in km s⁻¹.

$$N_{HI} = 1.823 \times 10^{18} T_S \int \tau_{\nu}(V) dV$$

$$N_{HI} = 1.823 \times 10^{18} \int T_B(V) dV$$
(2.23)

The spin temperature (T_S) is expressed as,

$$T_S = \frac{N_{HI}}{1.823 \times 10^{18} \int \tau_{\nu}(V) dV}$$

$$\Rightarrow T_S = \frac{\int T_B(V) dV}{\int \tau_{\nu}(V) dV}$$
(2.24)

In this study of HI 21-cm absorption, the column density ($N_{\rm HI}$) is calculated using HI 21-cm emission spectra obtained from the LAB (Leiden/Argentine/Bonn) Galactic HI Survey². The observed intensity is measured in terms of the brightness temperature (T_B), and the steps described above are followed to determine $N_{\rm HI}$. For the calculation of the spin temperature (T_S), we use the emission spectra along with the corresponding absorption spectra obtained against background continuum sources along nearby sightlines, as described in Chapter 3.

²https://cade.irap.omp.eu/dokuwiki/doku.php?id=lab

When the gas along the sightline is not homogeneous and exhibits variations in density and temperature, the derived spin temperature does not correspond to a single, uniform component. Instead, from Eq. 2.24, we obtain the column-density-weighted harmonic mean spin temperature, denoted by $\langle T_S \rangle$. Owing to the presence of density and temperature variations both along and transverse to the line of sight, many studies employ multi-Gaussian fitting to the absorption spectra. From the widths of the fitted components, one can infer the kinetic temperature of each component, assuming that the line broadening is purely thermal. However, in practice, this method provides only an upper limit on the temperature, since non-thermal processes such as turbulence within the Galaxy or differential rotation of the gas can also contribute to line broadening. By decomposing the spectra into individual components, it is also possible to estimate the column density and spin temperature for each component separately. This approach was adopted by Roy 2013b and Patra 2024 to understand and verify observational indications of a significant fraction of neutral gas in the interstellar medium (ISM) residing in the thermally unstable region.

Chapter 3

Observational Techniques

3.1 Introduction

Neutral hydrogen (HI) in the interstellar medium (ISM) exists in different thermal phases, primarily the cold neutral medium (CNM) and the warm neutral medium (WNM). While the CNM can be readily detected through HI 21cm absorption due to its high optical depth, the WNM—being warmer and more diffuse—produces much weaker absorption signatures, making its detection challenging. Understanding the physical properties of the WNM is crucial for a complete picture of the ISM, yet it remains relatively poorly constrained observationally. This study aims to probe the WNM by conducting a deep HI 21cm absorption survey using the upgraded Giant Metrewave Radio Telescope (uGMRT). This work is part of a larger effort to build a statistically significant sample of compact radio-loud background sources suitable for HI absorption studies. Previous analyses by Roy 2013b, Patra 2018, and Patra 2024 have covered subsets of this sample using the GMRT and the Westerbork Synthesis Radio Telescope (WSRT). The current study focuses on the remaining 12 sources observed with the uGMRT, which offers improved sensitivity and spectral resolution.

The following sections describe the sample selection, observational strategy, data analysis methods, and the results of the survey, with particular emphasis on detecting weak WNM absorption features.

3.2 The sample

An HI absorption survey was conducted using GMRT and WSRT towards a large number of sources, aiming to detect absorption by WNM in order to understand the physical condition of this phase better. The initial sample consisted of 54 compact radio sources, which are the VLA calibrators¹. These calibrators have L-band flux density greater than or equal to 3Jy; bright sources are chosen to detect absorption. From this sample, 30 sources observed from GMRT (10) and WSRT (20) were analysed by Roy 2013b and Patra 2018, then 12 sources observed from WSRT were analysed by Patra 2024. The remaining 12 sources from the total sample observed from the uGMRT are analyzed in this study.

3.3 Observation

The uGMRT observations of this sample, consisting of 12 sources, were conducted using two different spectral configurations. For 10 of the sources, a baseband bandwidth of 6.25 MHz was used, divided into 8192 channels, resulting in a velocity resolution of approximately 161 m/s. The remaining two sources were observed with a baseband bandwidth of 6.242 MHz, divided into 16,384 channels, yielding a higher velocity resolution of 80.46 m/s. The total observation time for each of the 10 sources was approximately 10–12 hours, while the two high-resolution sources were observed for around 30 hours each.

The standard procedure for bandpass calibration was not used in these observations, as it proved ineffective for two key reasons. First, any calibrator source chosen is contaminated by Galactic HI emission or absorption. By using such a source for bandpass calibration, we will not be able to detect absorption weaker than that present in the calibrator. The absorption features will be treated as instrumental effects and will be effectively "corrected out," which compromises the scientific goal of this study of detecting weak absorption lines. The objective of bandpass calibration is to characterize the frequency response of the system, not to remove astrophysical signals.

https://science.nrao.edu/facilities/vla/observing/callist

Second, since the target sources themselves are strong continuum sources (in fact, VLA calibrators), selecting a separate bandpass calibrator would require more observational time to achieve a comparable signal-to-noise ratio. To address these issues, a frequency-switching calibration method was employed.

A detailed study of the frequency-switching technique using the GMRT was conducted by Roy and Nissim Kanekar 2007, who concluded that switching at the first local oscillator (LO) yields a flat spectral baseline. Accordingly, for uGMRT observations, bandpass calibration is performed using frequency switching at the first LO, typically every 5 minutes, with a frequency throw of 2 MHz, ensureing that the frequency region of interest remains within the observing band.

3.4 Data Analysis

An interferometer (such as the GMRT, shown in Fig. 3.1) consists of an array of antennas that together behave like a single, large antenna. Each individual antenna receives the incoming electric field from a source, which is then transmitted via electronic chains to a central correlator. The correlator computes the visibility. This measured quantity is referred to as the observed visibility (V^o), as it has been modified by instrumental and environmental effects and thus does not represent the true visibility (V^T). These modifications include complex gain factors introduced by the electronic system, as well as atmospheric and ionospheric distortions. All such effects can be encapsulated in complex gain terms. In a loose notation, the relationship between observed and true visibilities can be understood as $V_{ij}^0 = G_i G_j^* V_{ij}^T + \text{noise}$, where V_{ij}^0 is the observed visibility corresponding to a single baseline, V_{ij}^T is the true visibility corresponding to a single baseline, and G_i is the complex gain term corresponding to each antenna (30 for GMRT). Our goal in data analysis is to flag the bad data and compute the true visibility.

In data analysis, before performing calibration, the data must first be flagged to remove bad or corrupted measurements. This includes data affected by terrestrial radio frequency interference (RFI), satellite signals, or from antennas that were malfunctioning during the observation. After this



Figure 3.1: Giant Meterwave Radio Telescope (GMRT)

cleaning step, we obtain a more reliable set of visibilities. The next step is calibration, which aims to recover the true visibility from the observed visibility by correcting for instrumental and atmospheric effects. This is done using calibrator sources — well-studied astronomical objects whose flux and structure are known from decades of observations across time and frequency. Calibration generally involves four major steps: flux calibration, delay calibration, gain (or phase) calibration, and bandpass calibration. A typical GMRT observing sequence is shown in Fig. 3.2. It begins and ends with short scans of a flux calibrator, while the target source is observed for the majority of the time. In between, scans of a phase calibrator are included at regular intervals to track time-dependent gain variations. Flux calibration corrects for errors in the measured flux scale. By observing a known flux calibrator at the start and end of the session, we compute a gain factor that is applied to the target source. Delay calibration accounts for signal delays caused by differences in cable lengths connecting each antenna to the correlator. Gain (or phase) calibration uses a nearby phase calibrator observed between target scans to correct for time-dependent changes in instrumental and ionospheric phases. Proximity to the target is important to ensure similar ionospheric conditions. Bandpass calibration corrects for frequency-dependent variations in the system response. This is also done using the flux calibrator generally, and the solution is interpolated across frequencies. Since the gain varies with time, we cannot apply a single cor-

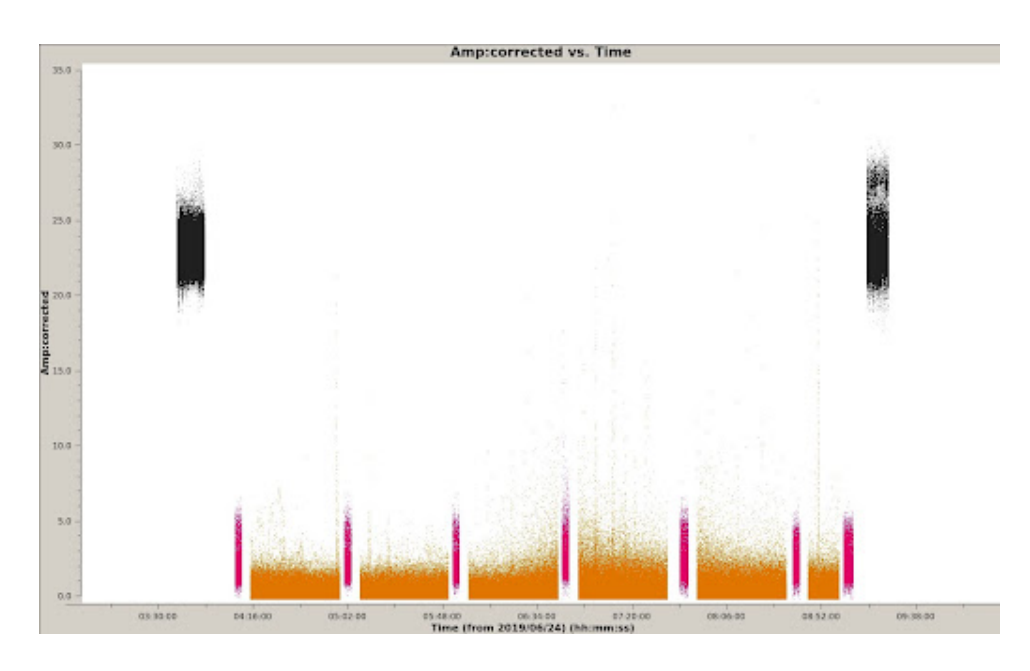


Figure 3.2: Amplitude v/s time plot (from CASA) for a standard GMRT observation

rection to the entire observation. Instead, we interpolate between calibration scans, which is why calibrators are observed frequently — to track variations and apply accurate corrections throughout the dataset. For our observation (shown in Fig.3.3), the phase calibrator is used as the bandpass calibrator. Due to the frequency-switching procedure, we have two spectral windows with the line in both regions. Therefore, bandpass calibration was performed by interpolating the solutions between the two spectral windows, described in section 3.3. Fig. 3.4 shows the two spectral windows after the flagging and calibration. The region of our interest (~ 1420MHz), is overlapping in both the spectral windows.

All the observational datasets were analysed using the GARUDA pipeline. It is based on the Common Astronomy Software Applications (CASA), an astronomical data reduction tool that can be run through an IPython interface. GARUDA uses a deep learning algorithm for RFI flagging. The flagging and calibration steps are fully automated in the pipeline. The performance of the pipeline was tested and verified using multiple datasets.

For all the sources, most of the continuum flux remains in the compact component; we measure that for each source. After that, we perform a

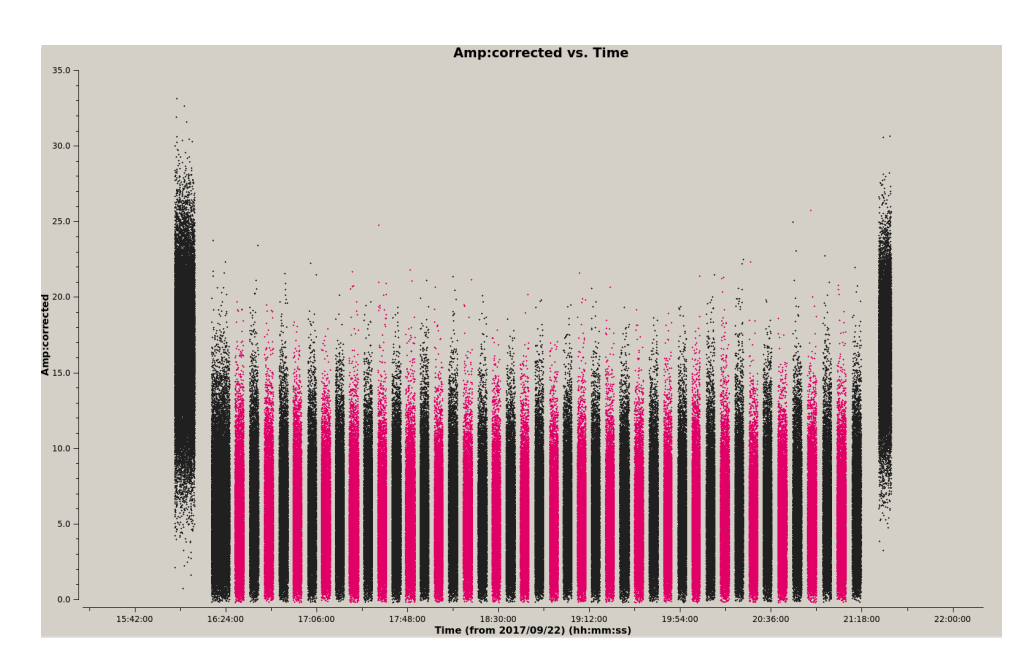


Figure 3.3: Amplitude v/s time plot (from CASA) showing the frequency switching observation for the source 0010-418. The two colors correspond to the two spectral windows (SPW0 $\sim 1415-1421$, SPW1 $\sim 1417-1423$)

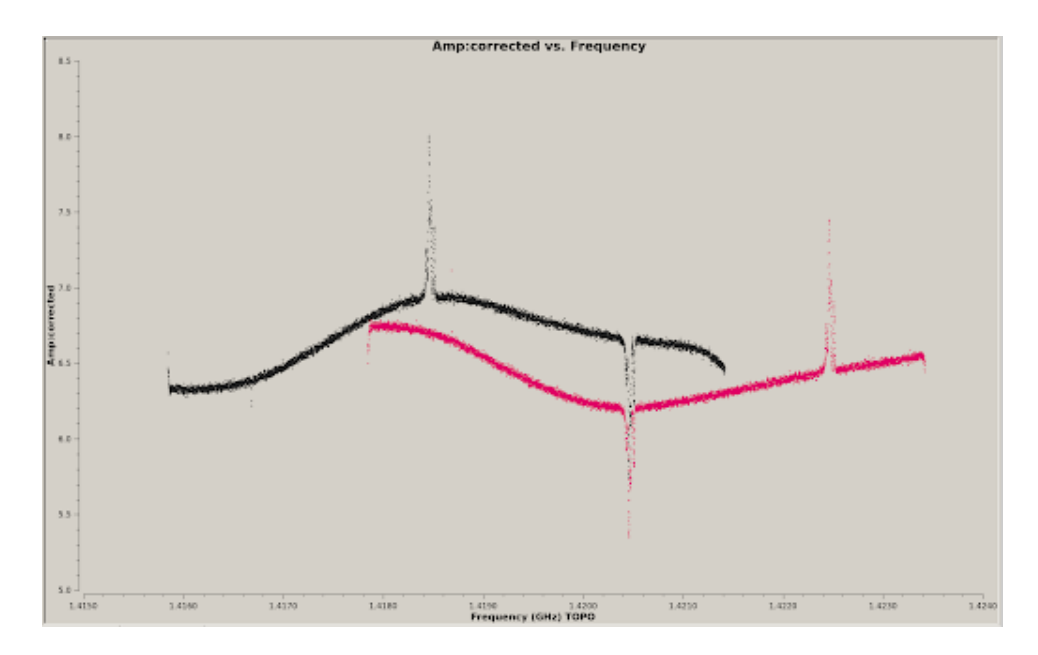


Figure 3.4: Amplitude v/s frequency plot (from CASA) after flagging and calibration. The plot shows the two spectral windows corresponding to two colours.

continuum subtraction on the line-free channels using the uvcontsub task in CASA, to get the visibility with just the absorption information. This residual u-v data is imaged in all the channels. We cut through this dirty cube to obtain the absorption spectrum for each source, where the x-axis represents the velocity in the local standard of rest (LSR) frame, and the y-axis shows the residual flux. Since we are observing point sources, we extract single-point profiles using imview task in CASA. We perform a baseband subtraction here to isolate the absorption dip, leaving behind just the noise. Using this data, we then compute the optical depth spectrum using the formula $I = I_0.e^{-\tau_{\nu}}$ in the optically thin limit, where I_0 is the flux density of the background source, estimated from the continuum image.

After fitting a polynomial of the appropriate order to our spectral line data for baseline subtraction, we check whether the residuals in the off-line region are consistent with noise. Since the noise in an instrument is due to various processes, it "tends" to have a Gaussian distribution as per the central limit theorem. To test this, we perform the Kolmogorov-Smirnov (K-S) test, which checks if our sample (noise region) is likely to have a Gaussian distribution. This test measures the maximum distance between the cumulative distribution function (CDF) of our sample and the Gaussian normal distribution; this distance is called the d-statistic. The main part of the test is to find the p-value, which is the probability of observing a value at least as significant as the d-statistic if our null hypothesis is true. The null hypothesis here is that the sample has the underlying Gaussian distribution. The p-values for all the sources suggest that the null hypothesis is correct. The d-statistic and the p-value are given in the Table 3.1.

We need to account for the error in the absorption spectrum. It has contributions from two factors: (1) n_c , the error in bandpass, due to issues like poor band stability, calibration errors, etc., and (2) n_b , the system temperature — it depends on the frequency-dependent sky brightness temperature; it is higher at certain frequencies (ν) where there is emission from HI galactic. At frequencies where there is no emission or absorption, these two components contribute equally to the noise, so $\sigma_{\text{off-line}} = \sqrt{n_c^2 + n_b^2}$. Therefore, $n_b = \frac{\sigma_{\text{off-line}}}{\sqrt{2}}$ and as it is independent of frequency, it will be constant. The component n_c will rise by the factor $\frac{T_{sky} + T_{sys}}{T_{sys}}$. The "frequency-

Name	d-statistic	p-value
2232+117	0.038	0.99
0010-418	0.065	0.96
1308-098	0.031	0.92
1130–148	0.033	0.86
2136+006	0.046	0.91
2130+050	0.072	0.28
0405-131	0.225	0.98
1326+319	0.033	0.96
0538-440	0.035	0.99
0745+101	0.039	0.83
0023-263	0.026	0.88
3C345	0.019	0.72

Table 3.1: Statistical parameters from the Kolmogorov–Smirnov Test evaluating the Gaussian nature of baseline residuals in off-line spectral channels for all observed sources

dependent sky brightness temperature" T_{sky} is obtained from the LAB (Leiden/Argentine/Bonn)² Galactic HI survey. T_{sys} for uGMRT is 70K. Final noise in any channel is estimated by $\sigma = \sqrt{n_c^2 + n_b^2}$. Here as the absorption spectra have higher velocity resolution, they have been resampled to the velocities of the LAB emission spectra.

²https://www.astro.uni-bonn.de/hisurvey/AllSky_profiles/index.php

Chapter 4

Results and Discussion

The physical conditions of different ISM phases are characterized by the spin temperature (T_S) and kinetic temperature (T_K) . The spin temperature quantifies the population ratio of the hyperfine levels in the ground state of neutral hydrogen. In a single, homogeneous HI cloud, T_S is determined by collisions, Ly- α coupling, and radiation near the 21-cm line. In highdensity phases like the cold neutral medium (CNM), collisions dominate, and $T_S \approx T_K$. In contrast, in the warm neutral medium (WNM), due to its low density, collisions are inefficient and $T_S < T_K$. However, actual sightlines have density and temperature variations along them. In such cases, we infer a column density-weighted harmonic mean spin temperature, which is biased toward the CNM because of its higher density, as discussed in Roy 2013a. A high inferred harmonic T_S may indicate that the gas is entirely in the WNM phase. Figure 4.1 (bottom panel) shows the spin temperature spectra, derived using Equation 2.20, where the observed uGMRT absorption spectra have been resampled to the LAB survey's velocity resolution. Red error bars mark HI 21-cm absorption detected with $\geq 3\sigma$ significance, and arrows denote 3σ lower limits. The emission and spin temperature spectra are at the LAB resolution of 1.03kms⁻¹, while the absorption spectra are at 161ms⁻¹ and 80.46ms⁻¹. The source name is shown at the top of each plot, and only the velocity range containing the absorption feature is displayed. For all of the sources, the spin temperature spectra have a value ($\geq 1000K$), which implies that the gas is almost entirely in the warm neutral region.

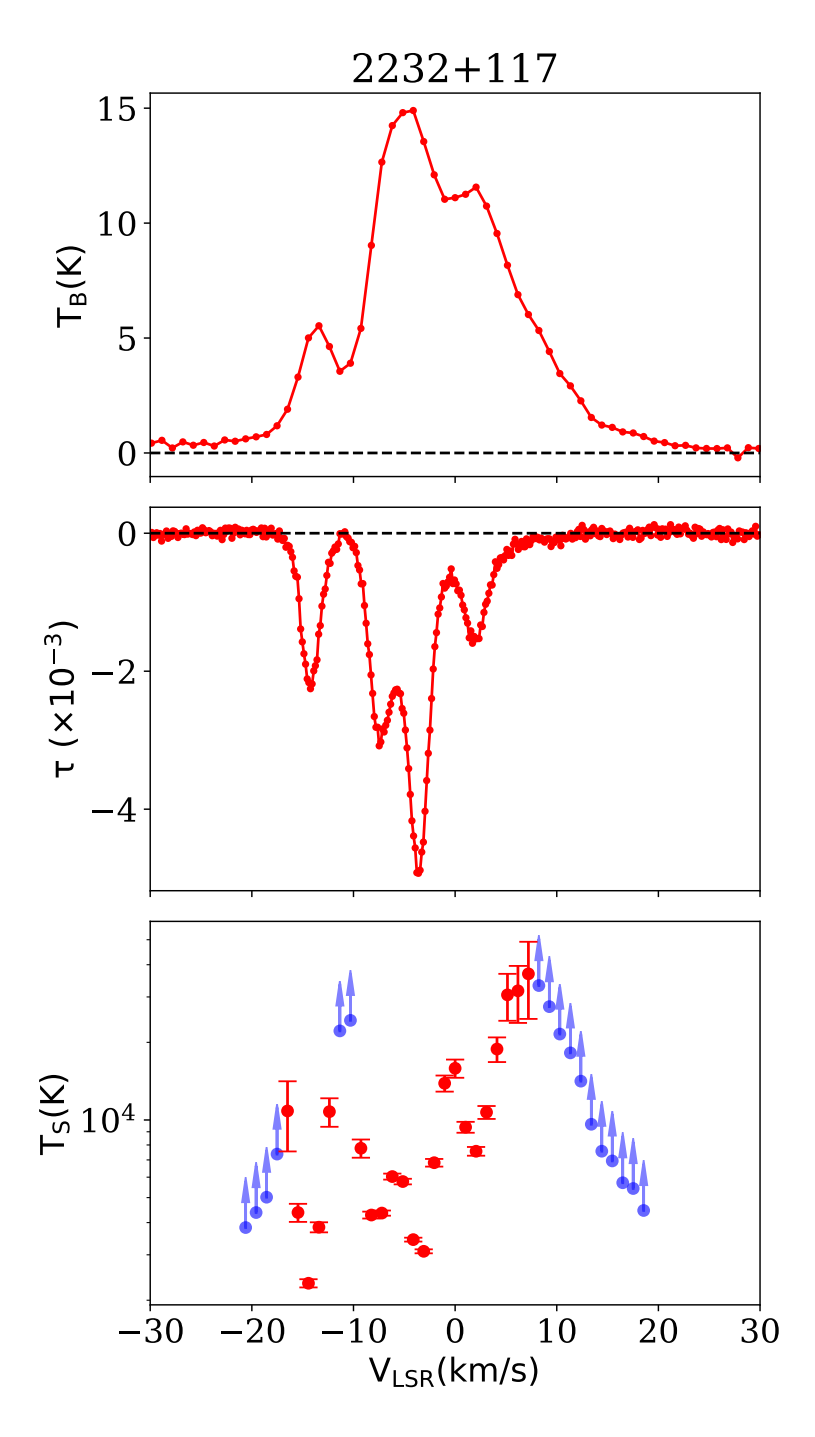


Figure 4.1: HI 21-cm absorption spectra obtained using the uGMRT. The top, middle, and bottom panels represent the 21-cm emission spectra (from the LAB Galactic survey), 21-cm optical depth spectra from our observation, and derived spin temperature spectra, respectively.

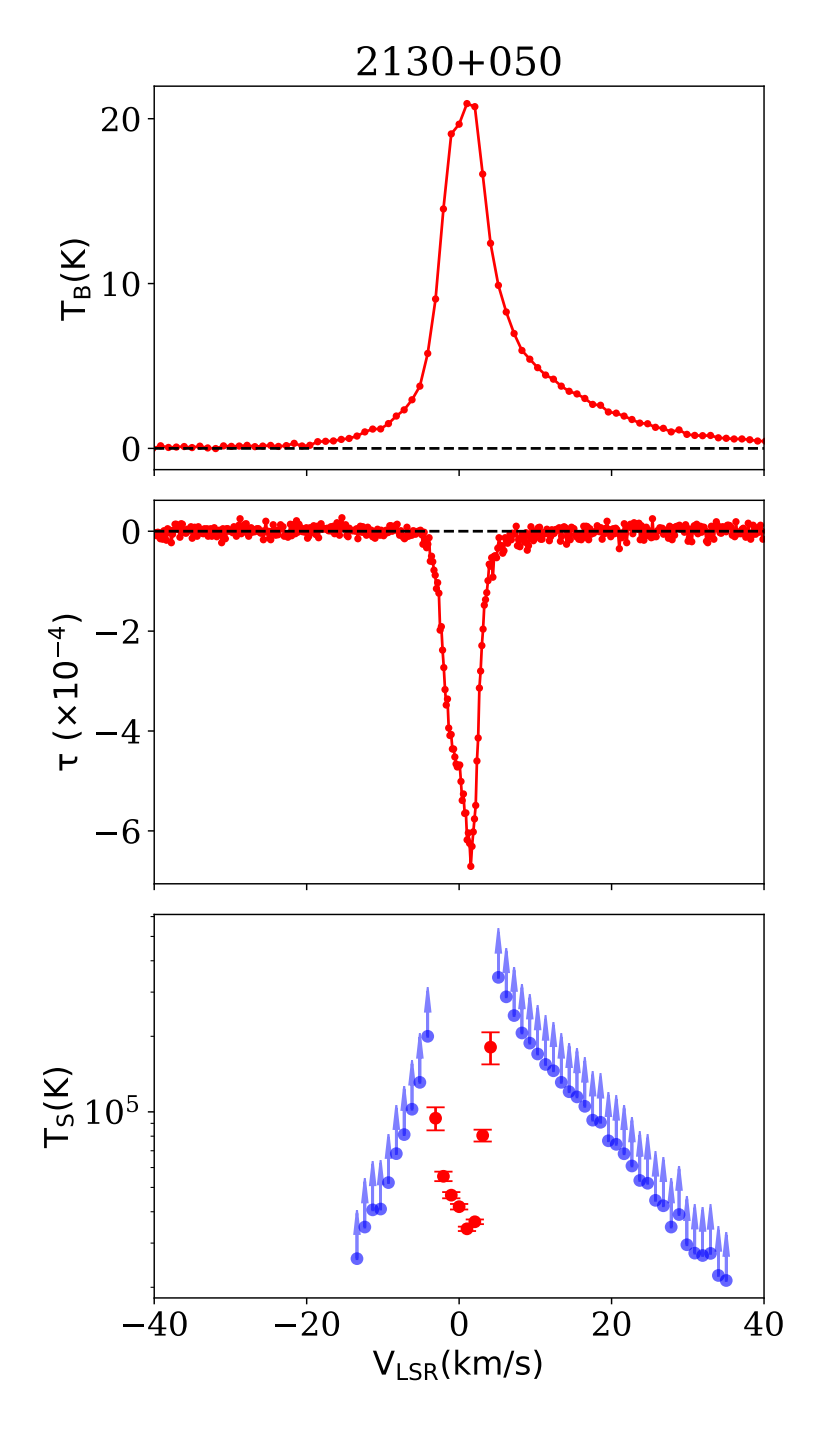


Figure 4.1: (Continued) HI 21-cm absorption, emission from LAB survey, and spin temperature spectra for source 2130.

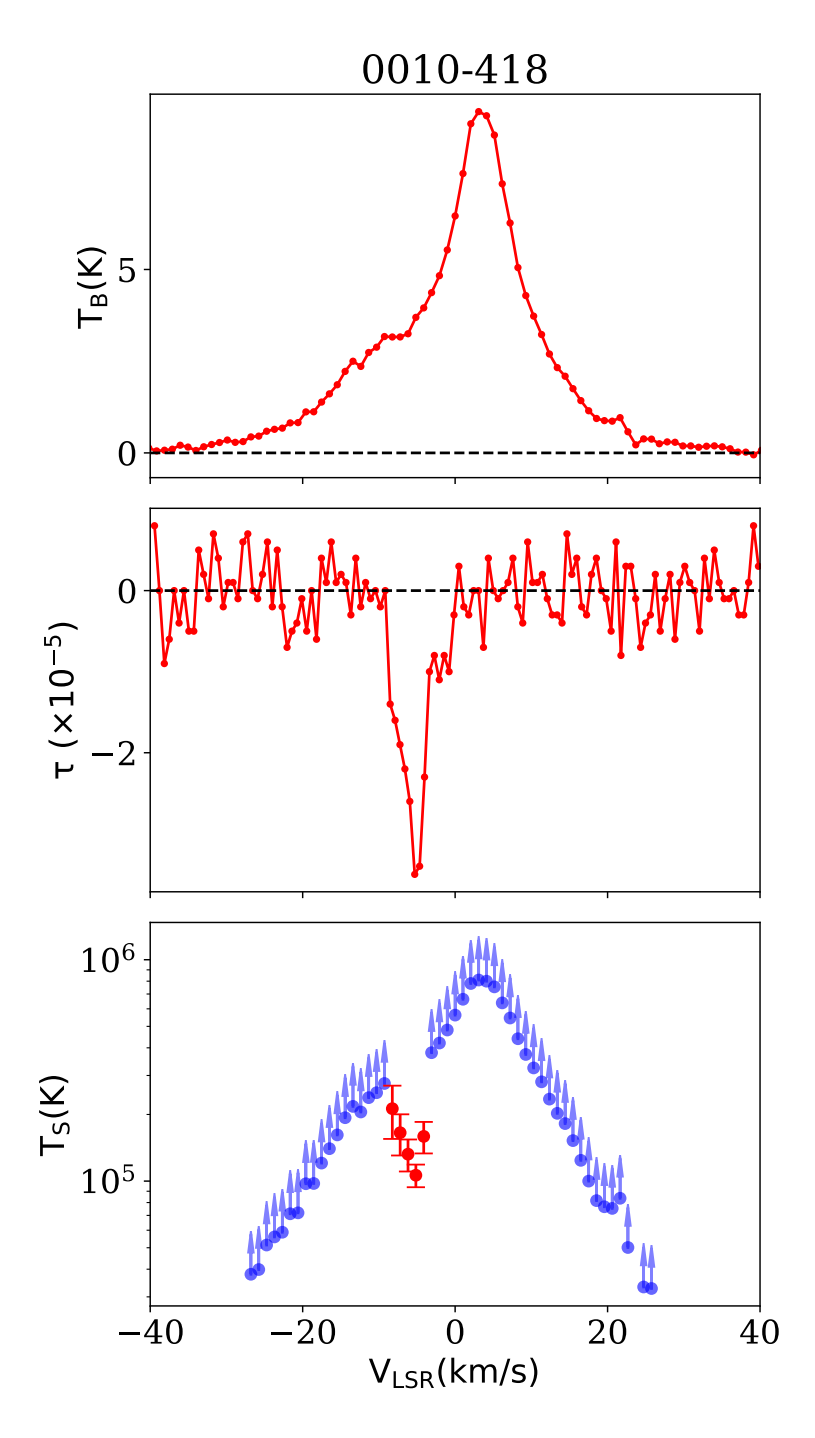


Figure 4.1: (Continued) HI 21-cm absorption, emission from LAB survey, and spin temperature spectra for source 0010.

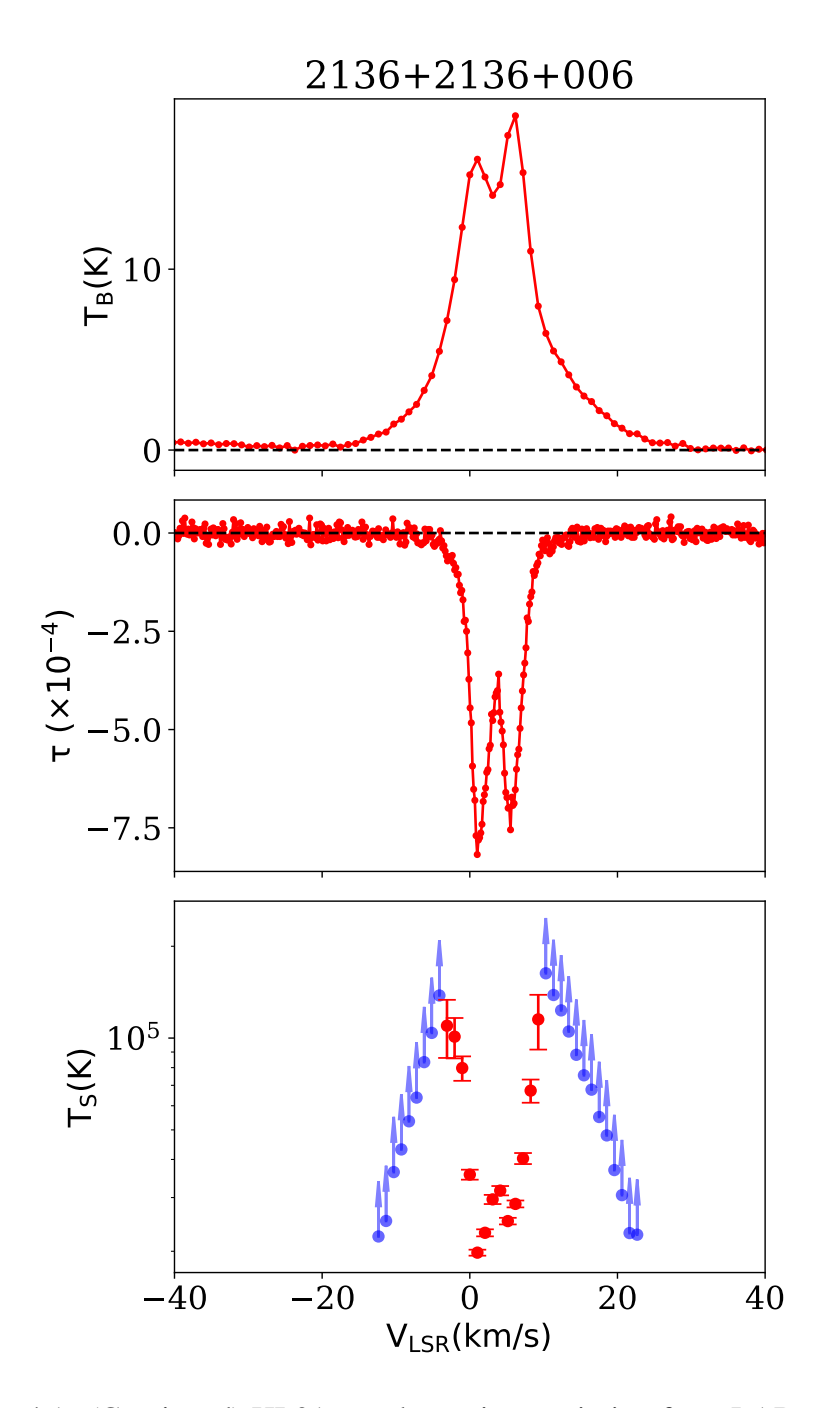


Figure 4.1: (Continued) HI 21-cm absorption, emission from LAB survey, and spin temperature spectra for source 2136.

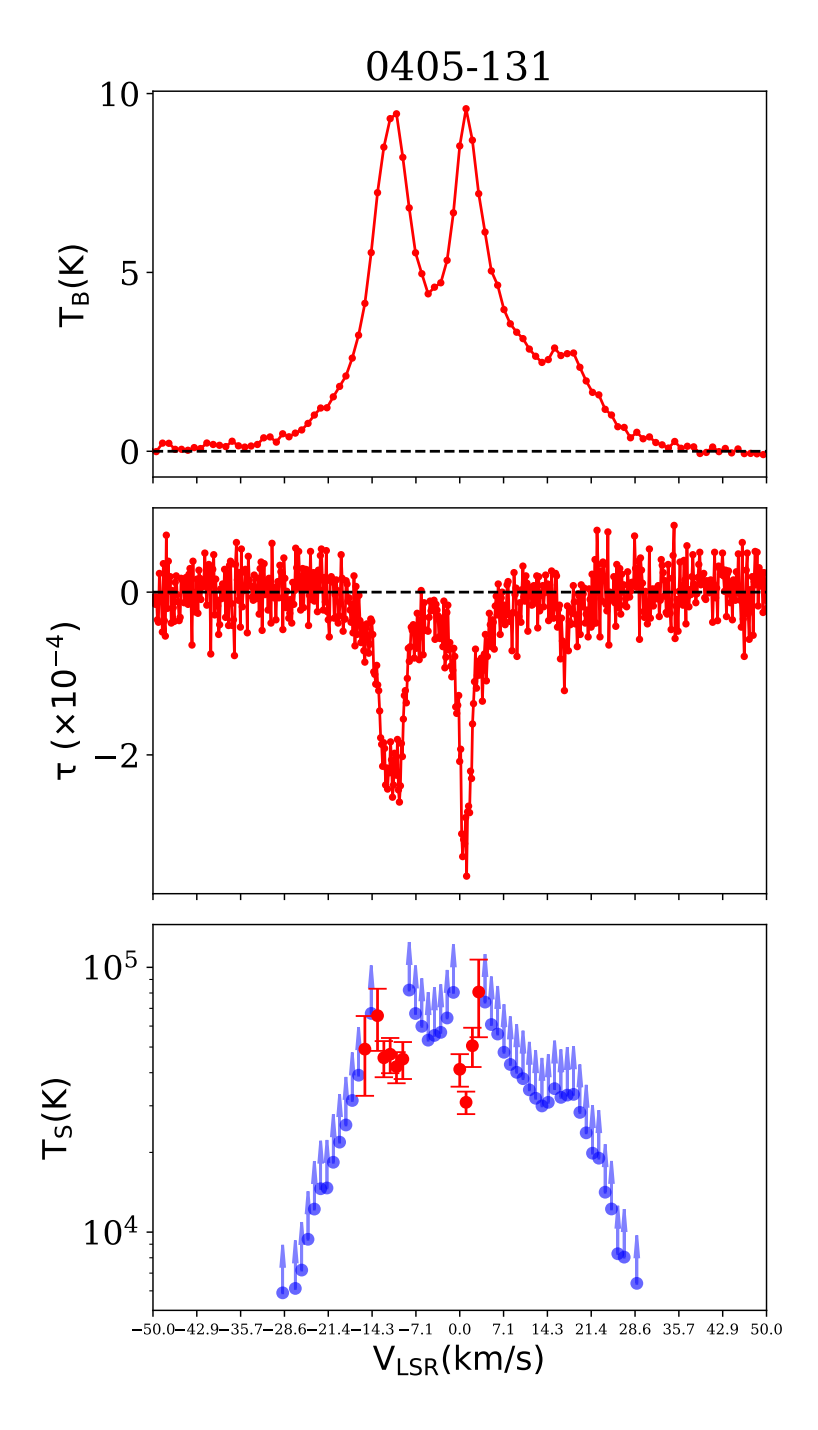


Figure 4.1: (Continued) HI 21-cm absorption, emission from LAB survey, and spin temperature spectra for source 0405.

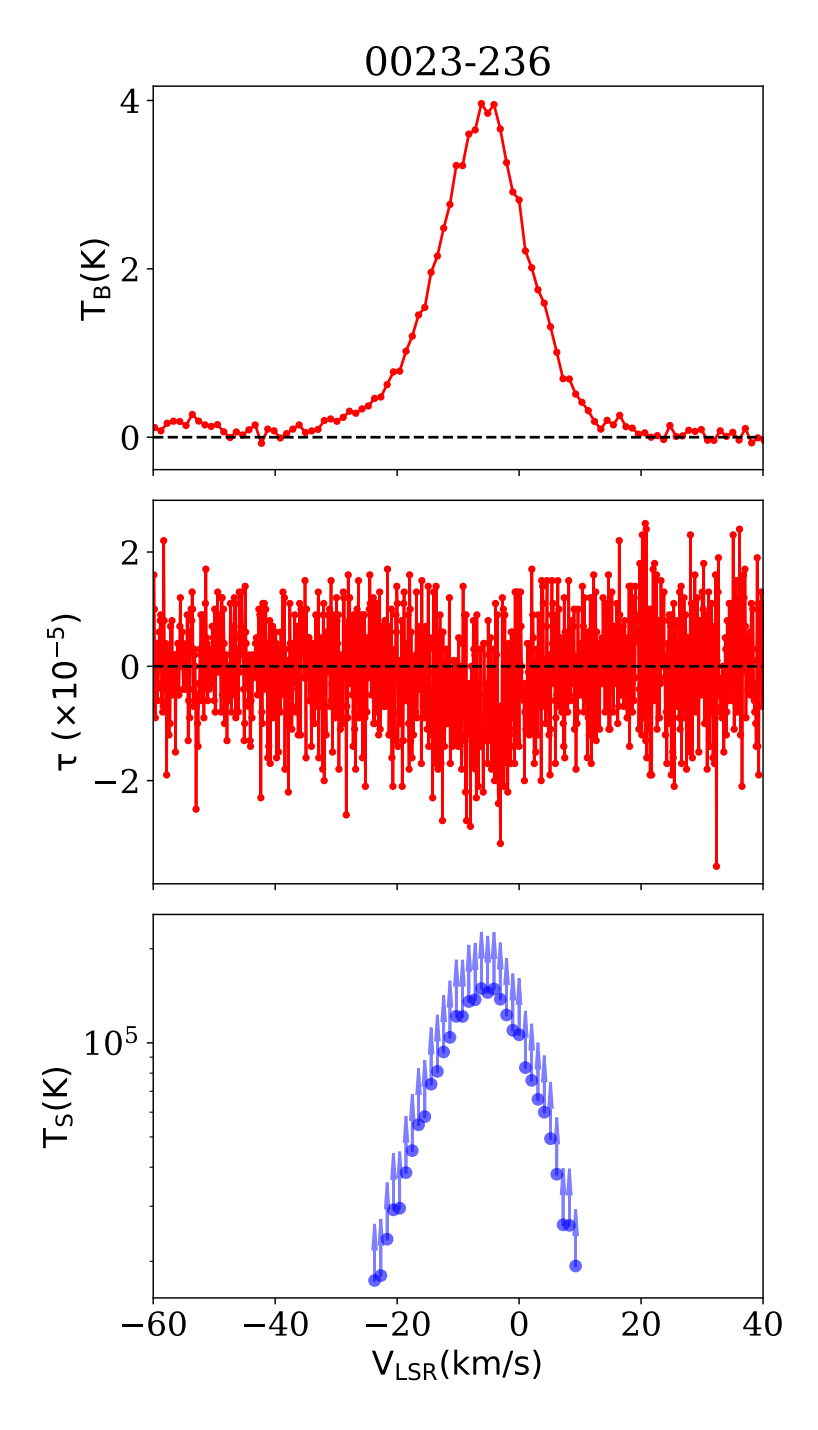


Figure 4.1: (Continued) HI 21-cm absorption, emission from LAB survey, and spin temperature spectra for source 0023.

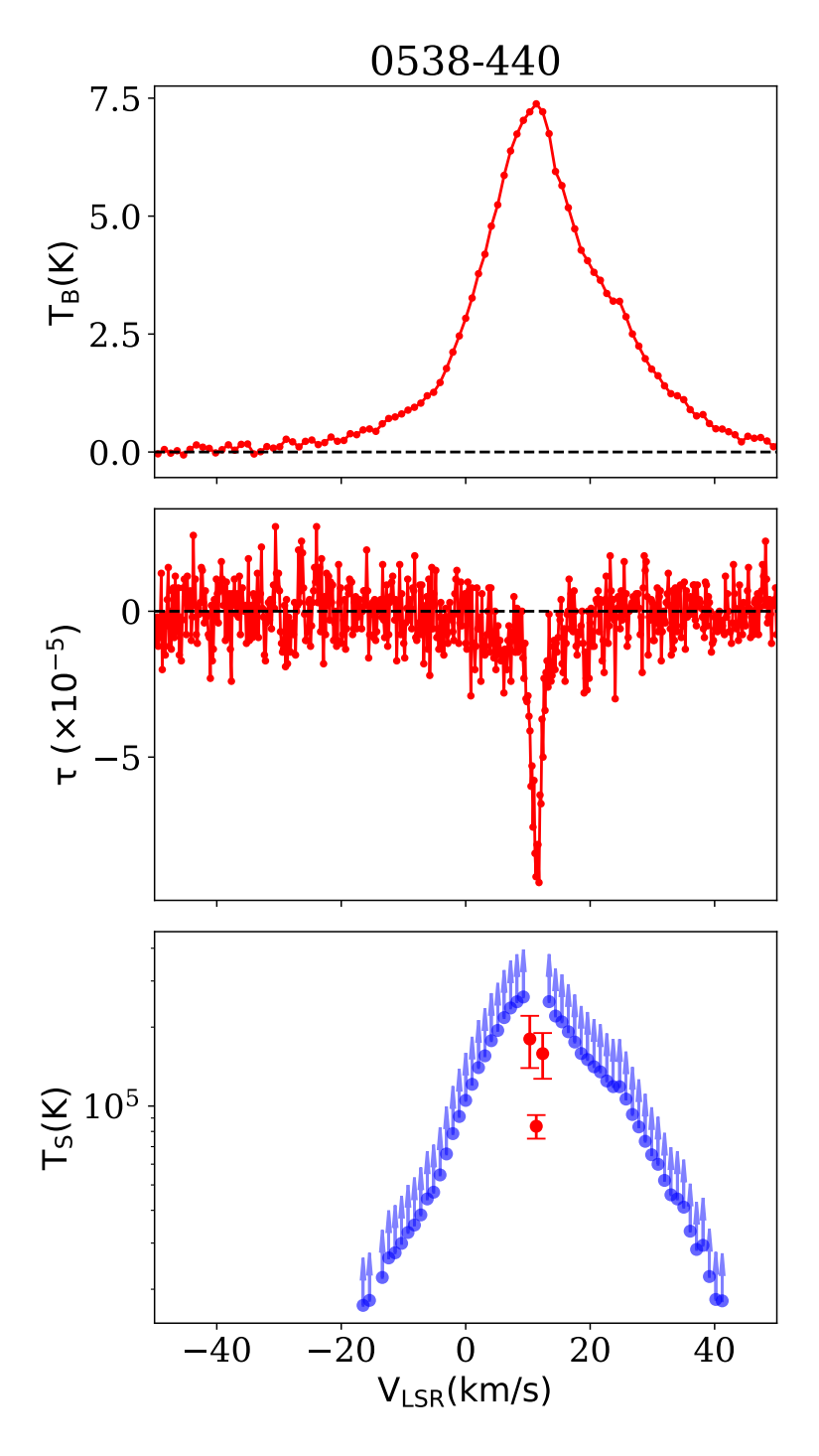


Figure 4.1: (Continued) HI 21-cm absorption, emission from LAB survey, and spin temperature spectra for source 0538.

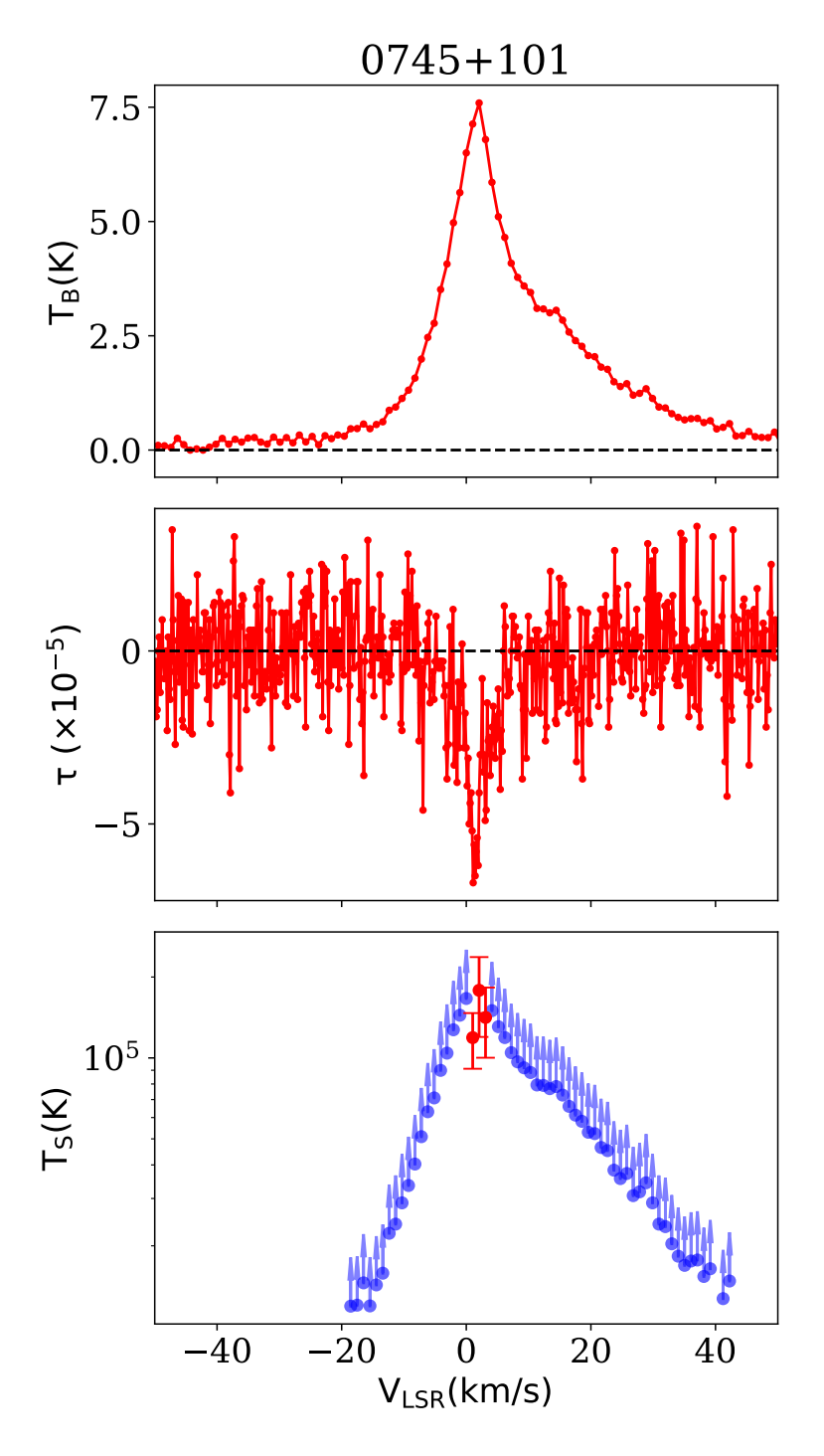


Figure 4.1: (Continued) HI 21-cm absorption, emission from LAB survey, and spin temperature spectra for source 0745.

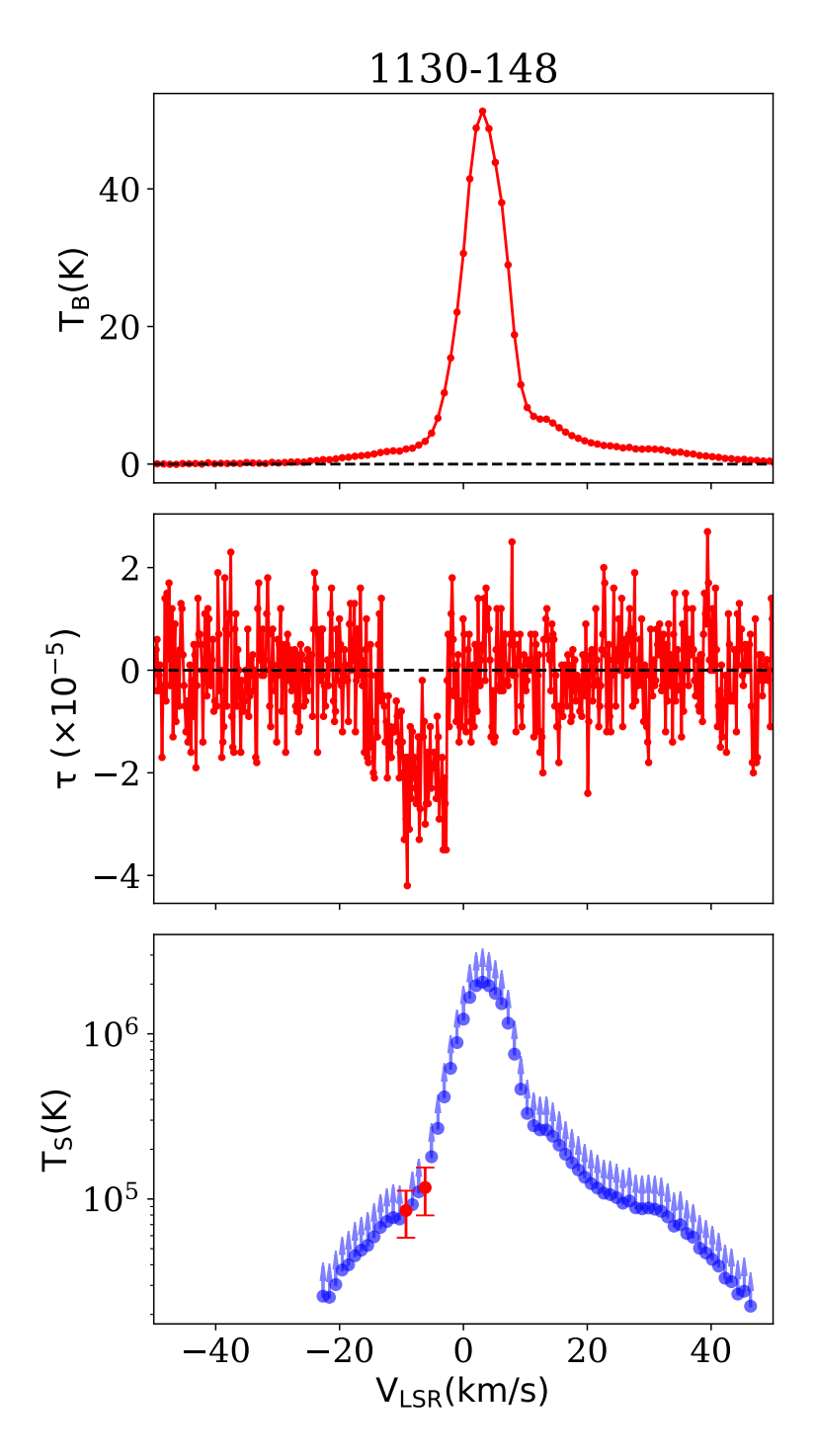


Figure 4.1: (Continued) HI 21-cm absorption, emission from LAB survey, and spin temperature spectra for source 1130.

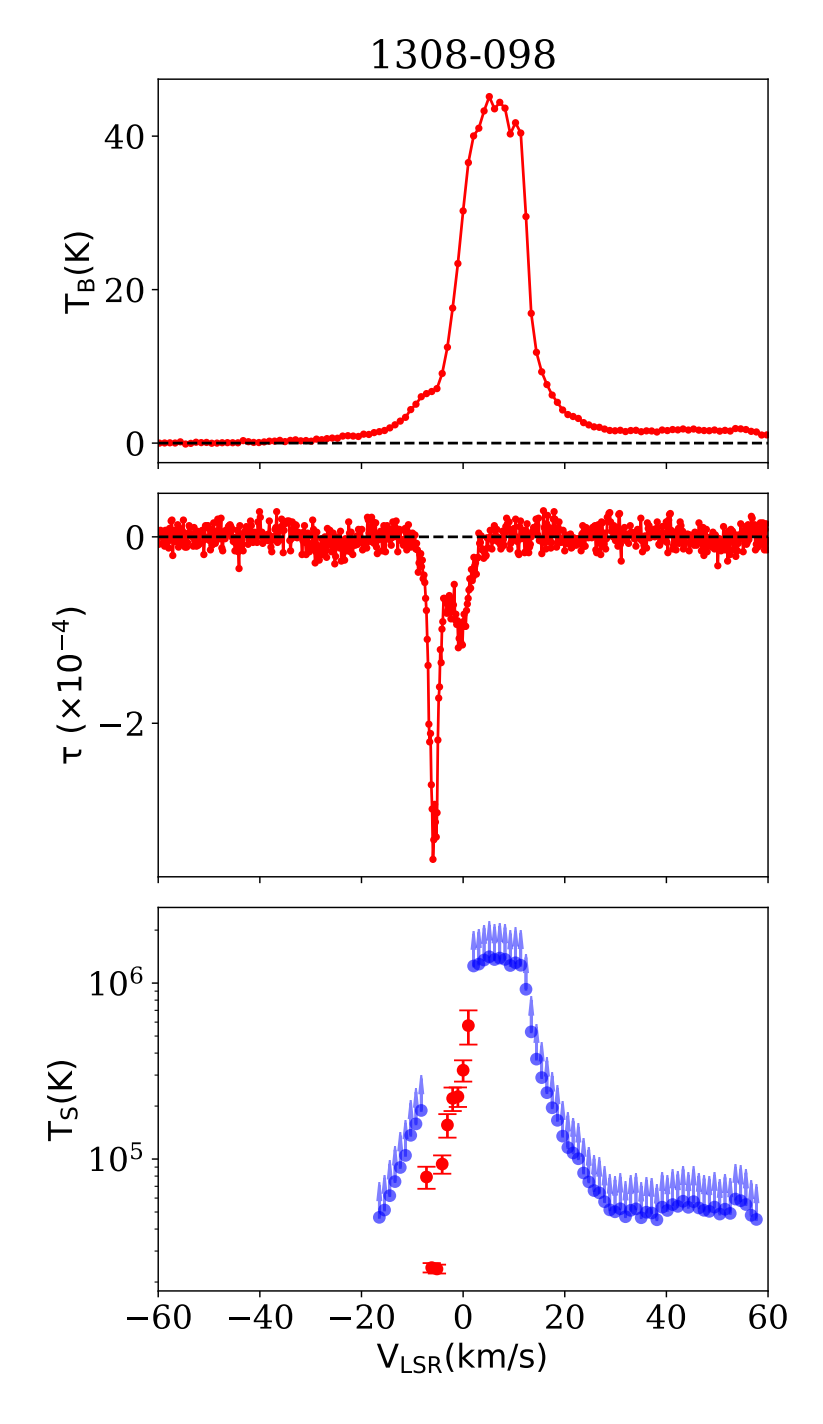


Figure 4.1: (Continued) HI 21-cm absorption, emission from LAB survey, and spin temperature spectra for source 1308.

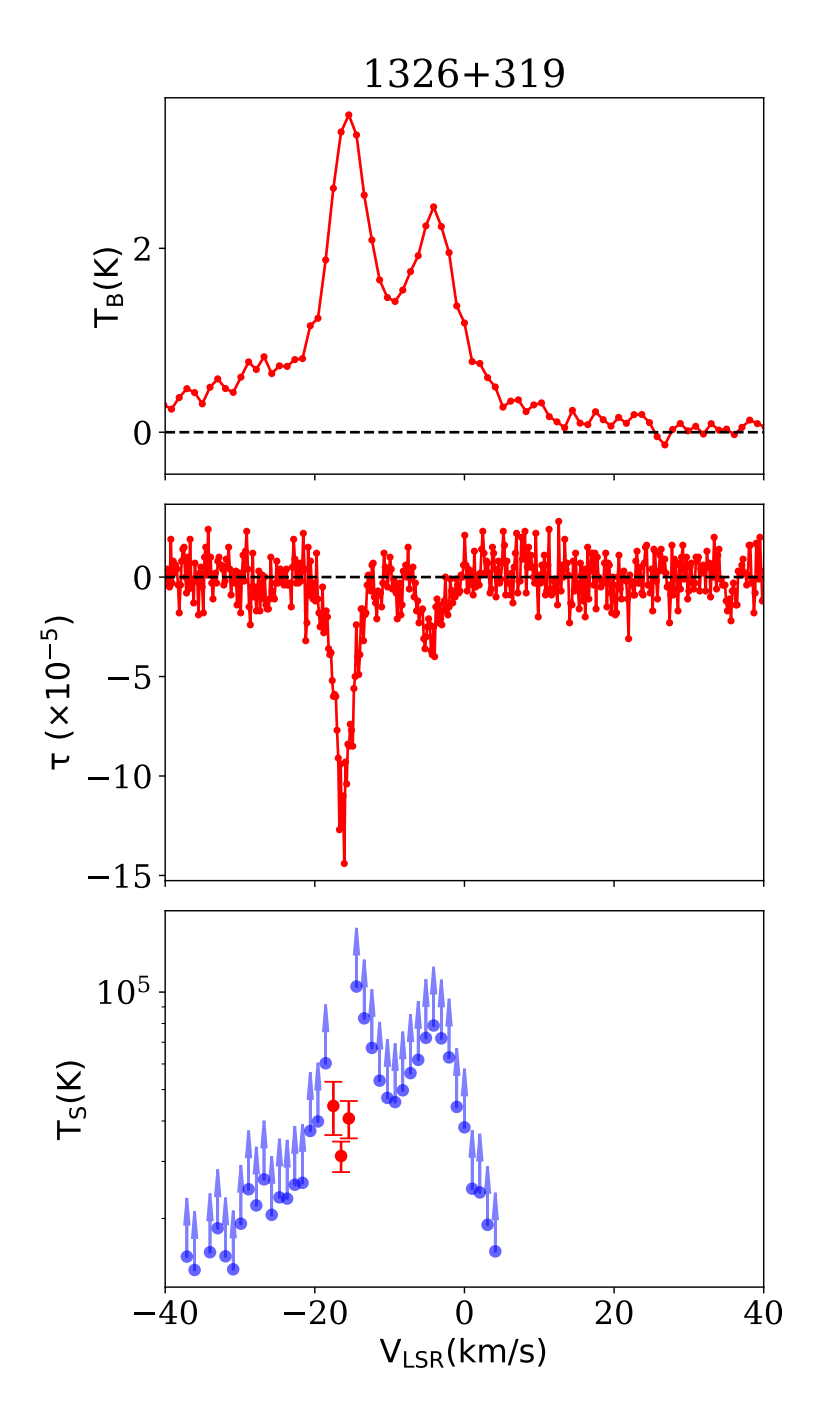


Figure 4.1: (Continued) HI 21-cm absorption, emission from LAB survey, and spin temperature spectra for source 1326.

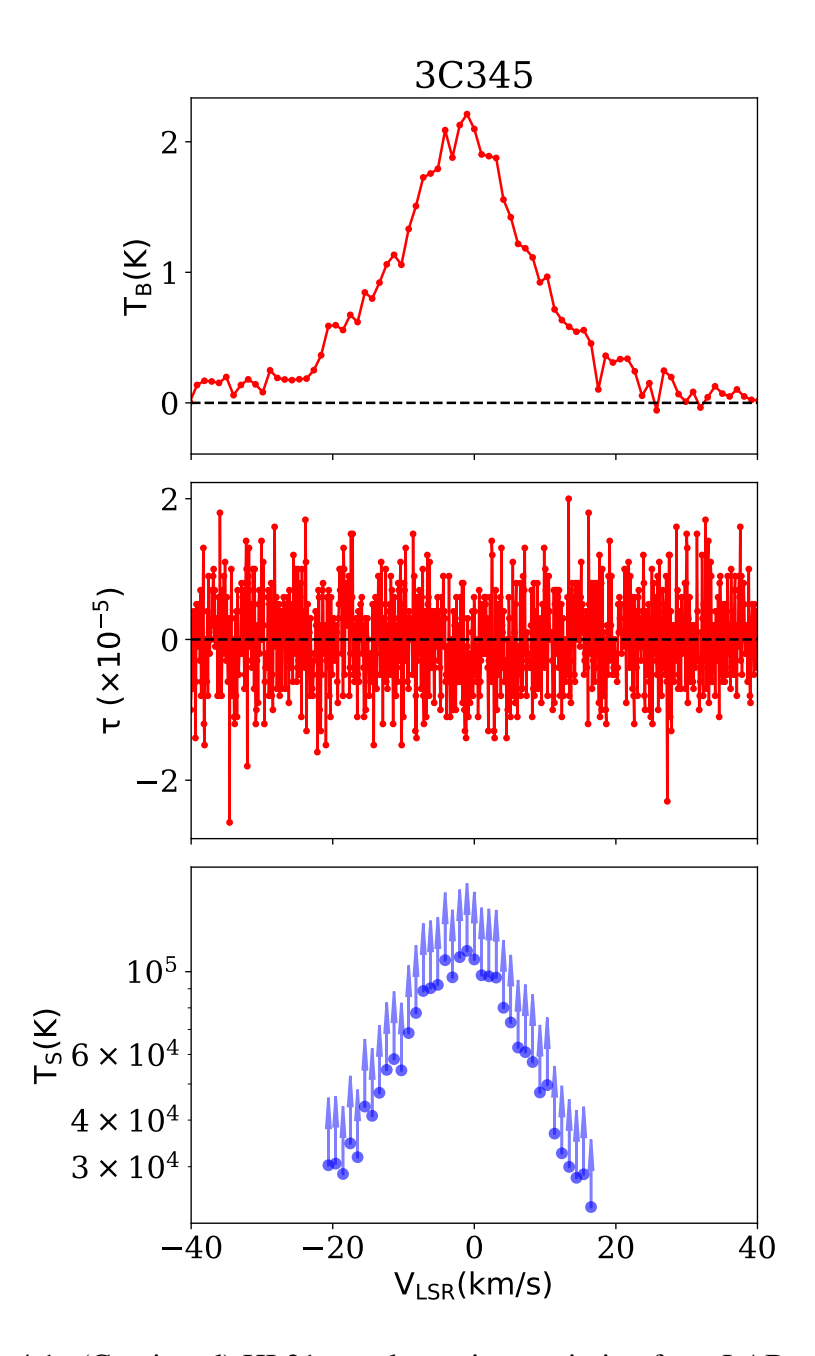


Figure 4.1: (Continued) HI 21-cm absorption, emission from LAB survey, and spin temperature spectra for source 3C345.

Name	S _{VLA} (Jy)	$\tau_{\rm rms}~(\times 10^{-6})$	$\tau_{\rm peak}~(\times 10^{-3})$	$\int \tau dv (\mathrm{km} \mathrm{s}^{-1})$	$N_{\rm HI}~(\times 10^{20}~{\rm cm}^{-2})$
2232+117	6.5	3.29	0.12	0.0342 ± 0.00013	4.7
0010-418	4.1	8.25	0.07	0.00028 ± 0.00004	3.0
1308-098	4.2	4.27	0.03	0.00127 ± 0.00003	14.5
1130-148	5.33	3.33	0.03	0.00021 ± 0.00001	10.4
2136+006	3.5	5.28	0.04	0.00533 ± 0.00003	4.5
2130+050	4.1	3.85	0.03	0.00291 ± 0.00002	4.7
0405-131	4.0	11.5	0.08	0.00293 ± 0.00008	4.0
1326+319	4.8	4.15	0.03	0.00047 ± 0.00002	1.2
0538-440	3.8	3.61	0.03	0.00035 ± 0.00002	3.2
0745+101	3.3	5.22	0.04	0.00030 ± 0.00020	2.8
0023-263	8.3	2.51	0.03	0.00010 ± 0.00002	1.4
3C345	8.0	1.92	0.02	0.00001 ± 0.00001	0.9

Table 4.1: Summary of observational results

In our observations, the optical depth spectra for nearly all sources have a root mean square (RMS) noise value of $\leq 10^{-6}$ per kms⁻¹ velocity channel, which is very sensitive to detect absorption by the warm neutral medium (WNM). This represents one of the best RMS values achieved so far. The details are presented in Table 4.1, where Columns 1 represent the source name, Column 2 shows the source flux density as listed in the VLA calibrator manual. Column 3 gives the RMS value measured in the line-free region of the optical depth spectra per kms⁻¹ channel. Column 4 lists the peak HI 21-cm optical depth, Column 5 the integrated optical depth, and Column 6 the HI column density along the line of sight.

Chapter 5

Conclusion

5.1 Summary

In this thesis, we aimed to conduct a high-velocity resolution HI 21-cm absorption study to detect absorption by the warm neutral medium (WNM). Due to the low optical depth of this phase of the interstellar medium (ISM), its detection has been challenging. The detection of broad absorption lines requires high-velocity resolution interferometric observations. Additionally, several studies have suggested that the temperature of the WNM lies in the thermally unstable range (e.g., Heiles and Troland 2003). Verifying this is important, as it challenges the theoretical models of the ISM that form the foundation of our current understanding. With this motivation, a larger project was initiated by Roy 2013b, comprising 54 sources to ensure statistically significant coverage of different sightlines. As part of this effort, a subsample of 12 sources observed with the upgraded Giant Meterwave Radio Telescope (uGMRT) was selected for the present study.

We analyzed uGMRT data for 12 lines of sight toward background continuum sources, using the GARUDA pipeline. After ensuring calibration and imaging the residual data, using the absorption spectra from our observations and the corresponding emission spectra from the LAB survey along nearby sightlines, the spin temperature spectra were obtained for all sources. Absorption was detected in all sources except for 3C345 and 0023-236, both of which have flux densities of approximately 8 Jy, as noted in the VLA

calibrator manual. We achieved an optical depth RMS noise level of approximately $\sim 10^{-6}$ per kms^{-1} , which is sufficient to detect absorption from the warm neutral medium. In comparison, earlier studies (e.g., Roy 2013a, Patra 2024) reported RMS values around $\sim 10^{-3}$ per kms^{-1} . Our results represent one of the best RMS sensitivities achieved to date. In all detected spectra, the peak spin temperature is $\geq 10^3$ K, indicating the presence of warm neutral gas.

5.2 Future Scope

Along a given sightline, the interstellar medium is not homogeneous—it exhibits variations in both temperature and density, not only along the line of sight but also transverse to it. These variations due to the presence of different phases along the sightline manifest as distinct features in the observed absorption spectra. Narrow components correspond to the cold neutral medium (CNM), while broader features are indicative of the warm neutral medium (WNM). To estimate the relative contribution of different phases, the absorption spectra are decomposed into multiple Gaussian components. This approach assumes that the line broadening is purely thermal. However, this assumption does not hold for the diffuse ISM, where nonthermal processes, such as turbulence, also play a significant role. The line can also have a Gaussian shape only when there is a contribution from a large number of non-thermal elements, such as turbulence in the ISM. Alternative approaches using non-Gaussian line shapes have been proposed (e.g., Braun and N. Kanekar 2005), but these also come with limitations and do not necessarily offer significant improvements over simple Gaussian fitting. Therefore, in this study, further analysis using multi-Gaussian decomposition can be applied to characterize the underlying ISM phases.

Bibliography

- Braun, R. and N. Kanekar (June 2005). "Tiny H I clouds in the local ISM". In: *Astronomy & Astrophysics* 436.3, pp. L53–L56. ISSN: 1432-0746. DOI: 10.1051/0004-6361: 200500122. URL: http://dx.doi.org/10.1051/0004-6361:200500122.
- Carilli (July 1998). "Detection of H I 21 Centimeter Absorption by the Warm Neutral Medium". In: *The Astrophysical Journal* 502.1, pp. L79–L83. ISSN: 0004-637X. DOI: 10.1086/311483. URL: http://dx.doi.org/10.1086/311483.
- Dickey, J. M. and F. J. Lockman (1990). "H I in the Galaxy". In: *Annual Review of Astronomy and Astrophysics* 28, pp. 215–261.
- Dwarakanath (Mar. 2002). "Detection of H I 21 Centimeter Line Absorption in the Warm Neutral Medium and in the Outer Arm of the Galaxy". In: *The Astrophysical Journal* 567.2, pp. 940–946. ISSN: 1538-4357. DOI: 10.1086/338755. URL: http://dx.doi.org/10.1086/338755.
- Ewen, H. I. and E. M. Purcell (1951). "Radio-Frequency Line Spectrum of Atomic Hydrogen in the Interstellar Medium". In: *Nature* 168. Discovery of the 21-cm line of neutral hydrogen, pp. 356–358. doi: 10.1038/168356a0. URL: https://ui.adsabs.harvard.edu/abs/1951Natur.168..356E.
- Ferrière, Katia M. (2001). "The interstellar environment of our galaxy". In: *Reviews of Modern Physics* 73.4, pp. 1031–1066. DOI: 10.1103/RevModPhys.73.1031.
- Hartmann, Johannes (1904). "Investigations of Spectral Lines in δ Orionis". In: *Astrophysical Journal* 19. Reprinted in Astrophys. J., 19, 268–274 (1904), pp. 268–274. DOI: 10.1051/0004-6361/200913796.
- Heiles, Carl and T. H. Troland (Apr. 2003). "The Millennium Arecibo 21 Centimeter Absorption-Line Survey. II. Properties of the Warm and Cold Neutral Media". In: *The*

- Astrophysical Journal 586.2, pp. 1067–1093. ISSN: 1538-4357. DOI: 10.1086/367828. URL: http://dx.doi.org/10.1086/367828.
- Jansky, K. G. (1933). "Electrical disturbances apparently of extraterrestrial origin". In: *Proceedings of the Institute of Radio Engineers* 21.10. First detection of cosmic radio waves, pp. 1387–1398. DOI: 10.1109/JRPROC.1933.227619. URL: https://ui.adsabs.harvard.edu/abs/1933Natur.132...66J.
- Kanekar, Nissim (Dec. 2003). "The temperature of the warm neutral medium in the Milky Way". In: *Monthly Notices of the Royal Astronomical Society* 346.4, pp. L57–L61. ISSN: 1365-2966. DOI: 10.1111/j.1365-2966.2003.07333.x. URL: http://dx.doi.org/10.1111/j.1365-2966.2003.07333.x.
- Kulkarni, Shrinivas R. and Carl Heiles (1988). "Neutral hydrogen and the diffuse interstellar medium." In: ed. by K. I. Kellermann and G. L. Verschuur, pp. 95–153.
- McClure-Griffiths, Naomi M. (2023). *Atomic Hydrogen in the Milky Way: A Stepping Stone in the Evolution of Galaxies*. arXiv: 2307.08464 [astro-ph.GA]. url: https://arxiv.org/abs/2307.08464.
- Patra, Narendra Nath (May 2018). "Detection of the Galactic warm neutral medium in H<scp>i</scp> 21-cm absorption". In: *Monthly Notices of the Royal Astronomical Society: Letters* 479.1, pp. L7–L11. ISSN: 1745-3933. DOI: 10.1093/mnrasl/sly087. URL: http://dx.doi.org/10.1093/mnrasl/sly087.
- (2024). The temperature of the neutral Interstellar Medium in the Galaxy. arXiv: 2403.11653 [astro-ph.GA]. url: https://arxiv.org/abs/2403.11653.
- Roy, Nirupam (Jan. 2006). "A multiwavelength investigation of the temperature of the cold neutral medium". In: *Monthly Notices of the Royal Astronomical Society: Letters* 365.1, pp. L1–L5. ISSN: 1745-3925. DOI: 10.1111/j.1745-3933.2005.00114.x. URL: http://dx.doi.org/10.1111/j.1745-3933.2005.00114.x.
- (Oct. 2013b). "The temperature of the diffuse Hi in the Milky Way II. Gaussian decomposition of the H i-21cm absorption spectra". In: *Monthly Notices of the Royal Astronomical Society* 436.3, pp. 2366–2385. ISSN: 0035-8711. DOI: 10.1093/mnras/stt1746. URL: http://dx.doi.org/10.1093/mnras/stt1746.
- (Oct. 2013a). "The temperature of the diffuse Hi in the Milky Way I. High resolution Hi-21cm absorption studies". In: Monthly Notices of the Royal Astronomical Society

```
436.3, pp. 2352-2365. ISSN: 0035-8711. DOI: 10.1093/mnras/stt1743. URL: http://dx.doi.org/10.1093/mnras/stt1743.
```

Roy, Nirupam and Nissim Kanekar (2007). *Frequency-switched bandpass calibration at the GMRT*. NCRA Technical Report R00228. National Centre for Radio Astrophysics.

Wolfire (Apr. 1995). "The Neutral Atomic Phases of the Interstellar Medium". In: 443, p. 152. doi: 10.1086/175510.